A&A 371, 133–151 (2001)
DOI: 10.1051/0004-6361:20010316

Astronomy & Astrophysics

Mineral formation in stellar winds

II. Effects of Mg/Si abundance variations on dust composition in AGB stars

A. S. Ferrarotti and H.-P. Gail

Institut für Theoretische Astrophysik, Universität Heidelberg, Tiergartenstraße 15, 69121 Heidelberg, Germany

Received 1 December 2000 / Accepted 27 February 2001

Abstract. Galactic F and G dwarf stars show a considerable star-to-star scatter of their individual abundance ratios of Mg to Si. We study the consequences of such abundance variations on the composition of the dust mixture formed in the circumstellar dust shells if the stars enter the AGB stage of stellar evolution. From thermodynamic equilibrium condensation calculations for the abundant dust components we find: (i) For $1 \lesssim \epsilon_{\rm Mg}/\epsilon_{\rm Si} \lesssim 2$ a mixture of forsterite (Mg_2SiO_4) and enstatite ($MgSiO_3$) is formed which consumes all of the available Mg and Si, (ii) for $\epsilon_{\rm Mg}/\epsilon_{\rm Si} \lesssim 1$ enstatite and quartz (SiO_2) are formed, while (iii) for $\epsilon_{\rm Mg}/\epsilon_{\rm Si} \gtrsim 2$ forsterite and solid MgO are formed. According to observed Mg/Si abundance ratios, about 90% of all stars fall into the first category, about 10% of all stars seem to fall into the second category, and virtually no stars fall into the third category. For the range of observed Mg/Si abundance ratios $0.6 \lesssim \epsilon_{\rm Mg}/\epsilon_{\rm Si} \lesssim 1.5$ we have studied the formation of a multicomponent mixture of dust in circumstellar dust shells by calculating simple stationary wind models including the non-equilibrium condensation of enstatite, forsterite, quartz, solid iron, and solid MgO. The variation of the composition of the non-equilibrium mineral mixture with varying Mg/Si abundance ratio is studied. The mineral mixture found to be formed under non-equilibrium conditions is somewhat different from the chemical equilibrium composition, but follows the general trends found in equilibrium calculations. Particular emphasis is laid on stars with a low Mg/Si abundance ratio ($\lesssim$1) where quartz grains are shown to form a significant dust component which should also be detectable by the absorption bands of quartz in the IR.

Key words. circumstellar matter – dust – stars: mass-loss – stars: winds – stars: AGB and post-AGB

1. Introduction

All stars with initial masses $0.5 \lesssim M_* \lesssim 8\ M_\odot$ on the main sequence finally evolve through the AGB stage of stellar evolution, shortly before they become white dwarfs. During this stage of their evolution they loose mass at an extremely high rate by a stellar wind and they develop optically thick circumstellar dust shells by condensation of solid particulates in the outflowing gas. The element mixture in the photospheric layers of the star initially is oxygen rich with $\epsilon_{\rm C} < \epsilon_{\rm O}$, as on the main sequence. In this case the stars appear as Giants of spectral type M. According to observation, such stars form silicate dust grains in the outflow, and probably they also form some additional minerals. Stars with initial masses in the range $1.5 \lesssim M_* \lesssim 4.5\ M_\odot$ (e.g. Groenewegen et al. 1995) after a few thermal pulses on the AGB mix products of the nuclear burning processes in their centre to the surface during the "third dredge-up" process. They develop through spectral type S, where $\epsilon_{\rm C} \approx \epsilon_{\rm O}$, to spectral type C (sometimes also denoted as spectral type N) where $\epsilon_{\rm C} > \epsilon_{\rm O}$. According to observations, the carbon stars form soot and silicon carbide particles in their outflow, and probably some other solid compounds.

The chemical composition of the mineral mixture condensing in the cooling outflow is determined by the abundance of such elements, which (i) form very stable solid compounds which exist at temperatures of the order of 1000 K even at the low pressure conditions of circumstellar dust shells, and which (ii) are sufficiently abundant to form dust in such quantities that emission from this dust contributes in detectable amounts to the infrared emission from the dust shell. Besides the obvious compositional differences between the dominating dust components formed around Giants of spectral type M or C (silicates for M stars, solid carbon and SiC for C stars) which are governed by the considerable variation of the carbon to oxygen element abundance ratio during evolution along the AGB, there may be further variations in the chemical composition of the circumstellar dust due to abundance variations

Send offprint requests to: H.-P. Gail,
e-mail: gail@ita.uni-heidelberg.de

of the other dust forming elements. In this paper we consider the composition of circumstellar dust formed in the shells around giant stars of spectral type M, where the abundances of C and O are not yet significantly changed by the "third dredge-up" episodes.

Detailed abundance determinations for AGB stars with respect to those elements which form the main dust components in AGB stars of spectral type M seem not to be available. Of particular interest for the formation of dust around M-type stars are the abundances of the elements Si, Mg, and Fe and to some extent also of Al, Ca, and Ni. Fortunately the nuclear electric charges of these elements are big enough in order that the nuclei are not affected by nuclear processes in the stellar burning zones during stellar evolution up to and on the AGB, which involve charged particles. Temperatures in the burning zone are much too low for an efficient processing of Mg, Si, and Fe. Additionally, the lighter nuclei have low neutron capture cross sections such that the overall abundances of the light elements also are not significantly modified by the *s*-process operating on the thermally pulsing AGB. Further, the *s*-process consumes only a small fraction of the Fe to form the heavy *s*-process nuclei. This allows us to use abundance determinations for main sequence stars if we look for abundances of the *dust forming elements* on the AGB.

Systematic studies for element abundances of main sequence stars and their dependence on metallicity, involving large samples of stars, are available for galactical F and G stars. This range of spectral classes and associated main sequence stellar masses is narrower than the range of initial masses of the progenitors of AGB stars, which corresponds to main sequence stars of a spectral type ranging roughly from late K to B3 (Lang 1992). However, stars of the same metallicity, i.e. formed at roughly the same period of the chemical evolution of the galaxy, should have all been formed with the same initial chemical composition (and the same abundance variations, if such exist) irrespective of their initial mass. Thus we can consider the abundances of the dust forming elements in F and G type main sequence stars as representative (at the same metallicity) for the abundances of these elements in AGB stars. We refrain from the small metallicity gradients in the galaxy, which makes a simple age-metallicity assignment somewhat difficult.

Two particular useful studies for our purpose are the abundance determinations by Edvardson et al. (1993) and Chen et al. (2000) which give abundances for the elements in which we are mainly interested in for a rather big sample of stars. Their results show that the abundances of the dust forming elements show a rather systematic variation of the abundances of Si, Fe, Al, and Ca with metallicity and a scattering of the abundances of individual stars around the mean which, however, is small. One cannot expect drastic variations of the chemical composition of the dust mixture resulting from such limited abundance variations. An important exception is magnesium which seems to show a very large scattering of the Mg abundance for individual stars. This strong scattering of individual Mg abundances is in sharp contrast to a rather uniform Si abundance of all stars of the same metallicity. Since Mg and Si are the two most important components for the formation of silicate dust in M-type AGB stars, this may have severe consequences for the chemical composition of the dust formed by such stars.

Table 1. Abundances of some elements (by number relative to H) used in the condensation calculations. Last column shows solar system abundances for comparison

El.	$\epsilon_{\rm AGB\text{-}star}$	$\epsilon_{\rm solar}$
He	$1.04\,10^{-1}$	$9.75\,10^{-2}$
C	$2.33\,10^{-4}$	$3.55\,10^{-4}$
N	$2.52\,10^{-4}$	$9.33\,10^{-5}$
O	$6.87\,10^{-4}$	$7.41\,10^{-4}$

The studies of Edvardson et al. (1993) and Chen et al. (2000) indicate, that Mg/Si abundance ratios for most of the stars with population I and population II metallicities are evenly distributed in the interval $1 \lesssim \epsilon_{\rm Mg}/\epsilon_{\rm Si} \lesssim 1.5$. In this case sufficient magnesium is available to condense the silicon completely in some type of magnesium-silicate dust. A fraction of $\lesssim$10% of all stars with population I and population II metallicity, however, seems to show magnesium abundances less than their silicon abundances, in some extreme cases the Mg/Si abundance ratio seems to be as low as 0.6, while e.g. the Solar System Mg/Si abundance ratio as given by Anders & Grevesse (1989) is 1.08 and for the present interstellar medium the data of Snow & Witt (1996) show Mg/Si = 1.34. For Mg/Si abundance ratios less than unity, the Si cannot completely be bound in magnesium-silicates and some other dust species have to be formed. We shall show that in this case quartz is formed as an additional dust component.

In the present paper we consider the consequences that follow from large variations of the Mg/Si abundance ratio for the chemical composition of the dust in circumstellar shells of objects with an oxygen rich chemistry. S and C stars are not considered in this paper. The general principles of calculating non-equilibrium dust formation are discusses in the first paper of this series (Gail & Sedlmayr 1999, henceforth called Paper I).

The plan of this paper is as follows: in Sect. 2 we briefly discuss the element abundances in AGB stars, in Sect. 3. we consider the chemical equilibrium condensation in element mixtures with varying Mg/Si abundance ratios, in Sect. 4 we discuss our model for calculating non-equilibrium dust condensation, Sect. 5 presents results for the non-equilibrium dust mixture formed in stationary stellar winds, Sect. 6 briefly discusses some consequences for the IR spectra, and Sect. 7 contains some concluding remarks.

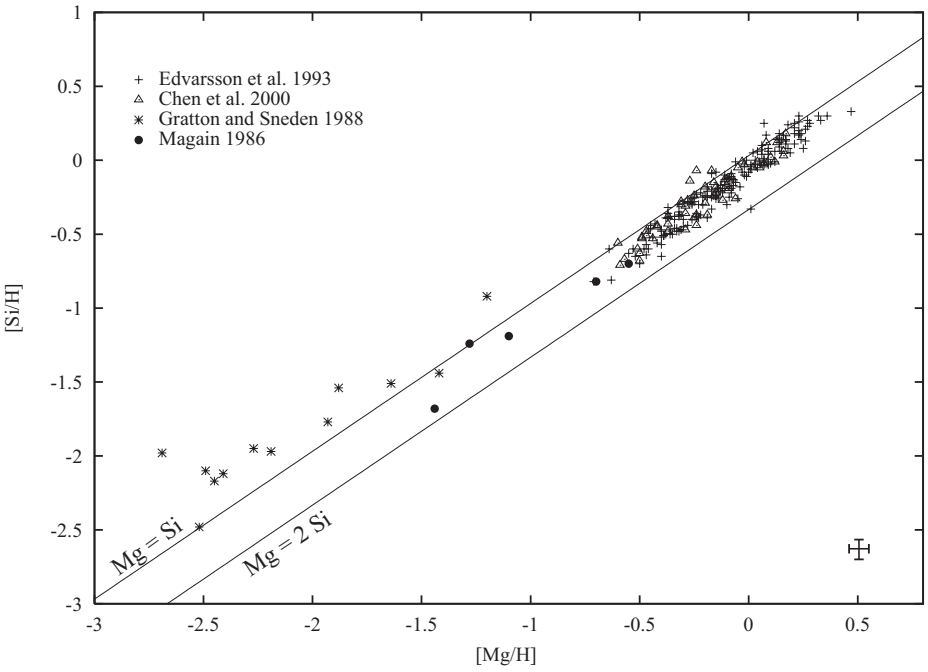

Fig. 1. Magnesium and silicon abundances in galactic F and G dwarf stars. The two lines correspond to $\epsilon_{\rm Mg} = \epsilon_{\rm Si}$ and $\epsilon_{\rm Mg} = 2\epsilon_{\rm Si}$ which bracket the Mg/Si abundance ratios for the coexistence of olivine and pyroxene dust. Stars with abundances above the upper limit line form no olivine dust but quartz and pyroxene dust. Stars with abundances below the lower limit line cannot form pyroxene but would form olivine and MgO dust. The cross in the lower right corner shows the estimated order of magnitude of the error of the abundance determinations by Edvardsson et al. (1993) and Chen et al. (2000)

2. Element abundances on the AGB

On the AGB the element abundances of the lightest and the heaviest elements significantly deviate from the abundances of these elements in the progenitor stars on the main sequence due to mixing of nuclear processed material from the burning zone to the stellar surface. The first and second dredge up processes at the bottom of the Red Giant Branch (first dredge up) and at the bottom of the Asymptotic Giant Branch (second dredge up) modify the abundances of He and of CNO by mixing material having burnt H to He by the CNO cycle into the stellar envelope. This slightly increases the He abundance. Since during H burning by the CNO cycle the inventory of C, N, and O nuclei is converted into the equilibrium isotopic mixture resulting from the CNO cycle, i.e. mainly into ^{14}N, mixing of such material to the envelope increases the N abundance and decreases the C and O abundances. After the second dredge up episode one expects a composition like that shown in Table 1. The "solar" values in the table correspond to the abundances given by Anders & Grevesse (1989) and Grevesse & Noels (1993). The "AGB" values are determined as follows: for He, C, N, and O we scaled the standard abundances according to the change in stellar surface abundances found in the evolutionary calculations of Schaller et al. (1992) for stars of small and intermediate masses. The CNO abundances determined in this way agree well with the observationally determined mean abundances of these elements in AGB stars as given by Smith & Lambert (1990, their Table 14).

As the star climbs up the AGB, at some instant the first thermal pulse occurs. At the same time third dredge up starts which mixes (i) freshly produced carbon from He burning and (ii) freshly produced *s*-process elements into the envelope. This converts after a few pulse cycles the chemistry of the stellar surface from an oxygen rich one into a carbon rich one for all stars whose initial masses are between $\approx$1 $M_\odot$ and $\approx$4.5 $M_\odot$. Stars with lower initial mass probably never become C-stars. More massive stars convert the carbon, which is mixed from the He burning zone into the bottom region of the outer envelope, via H burning by the CNO cycle into N (the "hot bottom burning" process) and retain their oxygen rich surface chemistry (cf. Lattanzio & Forestini 1999).

The abundances of nuclei with intermediate masses between the light nuclei participating in the CNO cycle and its side paths at one hand and the heavy nuclei beyond the iron peak on the other hand, are not affected by nuclear burning processes in AGB stars. Central temperatures in AGB stars are too low for proton capture to occur except for the lightest nuclei, and the medium mass nuclei up to about the iron peak have low neutron capture cross sections and do not participate in the *s*-process. This means that for the elements from Mg to Ni the abundances of the abundant isotopes are not significantly affected by nuclear processing on the AGB; these nuclei are mainly synthesised in supernovae. Only some rare isotopes undergo significant abundance changes, for instance the long lived unstable ^{26}Al isotope is formed (e.g. Forestini & Charbonnel 1997). The total abundances of the elements from Mg to Ni in AGB stars, thus, are nearly identical to their initial abundances at the time of formation of the progenitor star.

With respect to the formation of dust in the circumstellar shells of AGB stars only the following elements are of interest: C, N, O, Mg, Al, Si, S, Ca, Fe, and Ni, because only these are sufficiently abundant to participate in the formation of observable quantities of dust. Less abundant elements like Ti, V, Zr may be important for the formation of seed nuclei, however.

Abundance determinations of the elements Mg, Al, Si, S, Ca, Fe, and Ni for AGB stars are scarce. The recent study of Edvardsson et al. (1993) with the improvements by Tomkin et al. (1997) give abundances for the elements of interest for a large sample of galactic F and G dwarf stars. The study of Chen et al. (2000) give abundances of the relevant elements for a considerable number of additional F and G dwarfs. The only exception is the element S for which no abundance determinations are given, but sulphur probably plays no role for dust formation in M-stars (but may be important for C-stars). For the stars in common between the two studies we have used the data of Edvardsson et al. (1993) and Tomkin et al. (1997) since abundance differences for individual stars between the two sets of abundance determinations are quite small. The error in the abundance determination for individual stars in Edvardsson et al. (1993) has been estimated to be at most of the order of $\pm 0.05 \ldots 0.1$ dex and the errors in Chen et al. (2000) are of the same order of magnitude. The correlation between the abundance ratios [Si/H] and [Mg/H], which are of particular interest for the silicate dust formation, for the 235 stars from the studies of Edvardsson et al. or Chen et al. where Mg and Si abundances both are determined, is shown in Fig. 1.

Abundances for some very metal poor stars have been given by Gratton & Sneden (1988) and Magain (1987). The errors of the abundance determinations are, however, much bigger then in the above mentioned studies (up to 0.15 for Gratton & Sneden and up to 0.26 for Magain). Figure 1 shows the ratios [Si/H] and [Mg/H] for 18 very metal poor stars for comparison.

The composition of the main dust components in M-stars is determined by the abundances of the three elements Si, Mg, and Fe. The oxygen abundance in these stars is so much higher than that of Si, Mg, and Fe that the formation of oxide compounds is not limited by the amount of available O. Figure 1 shows the correlation between the abundances [Si/H] and [Mg/H] for 177 stars from Edvardsson et al. (1993) and Tomkin et al. (1997), 58 stars from Chen et al. (2000), 13 stars from Gratton & Sneden (1988), and 5 stars from Magain (1987). Additionally the figure shows the two lines where $\epsilon_{\rm Mg} = \epsilon_{\rm Si}$ and $\epsilon_{\rm Mg} = 2\epsilon_{\rm Si}$. As is clearly seen, for stars with population I and population II metallicities (the studies of Edvardsson et al. and Chen et al.) the abundance ratio $\epsilon_{\rm Mg}/\epsilon_{\rm Si}$ for most stars is strongly concentrated in the region $1.0 \leq \epsilon_{\rm Mg}/\epsilon_{\rm Si} \leq 1.5$. A small fraction of stars ($\lesssim$10%) have Mg abundances less than the Si abundance down to $\epsilon_{\rm Mg}/\epsilon_{\rm Si} \approx 0.6$. Only one star seems to show a Mg abundance slightly in excess of twice the Si abundance. As we shall see below, the two limits $\epsilon_{\rm Mg} = \epsilon_{\rm Si}$ and $\epsilon_{\rm Mg} = 2\epsilon_{\rm Si}$ correspond to limits where a change of the mineral composition of the circumstellar dust is to be expected.

For the very metal poor stars (the studies of Gratton & Sneden, Magain) the Mg abundance generally seems to be less than the Si abundance, in many cases even much lower. In the following these stars are not considered, since it is not clear whether they will form dust in their stellar wind if stars of such a low metallicity enter the AGB stage of stellar evolution.

The cross in the lower right corner of Fig. 1 shows the estimated maximum error of the abundance determinations according to Edvardsson et al. (1993) and Chen et al. (2000). The scatter in the Mg/Si abundance ratios considerably exceeds the errors in the abundance determinations. This indicates large individual star-to-star variations of the Mg/Si abundance ratio. Such variations might result, for instance, from strong variations with initial mass of the progenitor star of the Mg/Si abundance ratios in the ejecta of supernovae of type II (e.g. Thielemann et al. 1993) and incomplete mixing of interstellar material, or from varying contributions of material from supernovae of type Ia which is very Mg poor (e.g. Thielemann et al. 1993). The AGB giant stars which are descendants of such dwarf stars can be expected to show the same range of Mg/Si abundance ratio variations. Since this ratio determines the composition of the dust mixture in an AGB star dust shell, considerable compositional variations of the mineral mixture can be expected to occur.

3. Equilibrium condensation of dust

Dust condensation in circumstellar dust shells occurs under conditions far from a chemical equilibrium state. Nontheless, consideration of the equilibrium condensation process is useful to determine the most stable condensates, since these can be expected also to be the likely candidates for condensation in a non-equilibrium state. Thus, we start with a determination of the composition of the equilibrium mineral mixture if considerable deviations of the Mg/Si abundance ratio from its value of 1.075 for the standard cosmic element abundance occur.

3.1. Equilibrium condensation of Si–Fe–Mg compounds

The main dust components in AGB stars of spectral type M are those formed from the most abundant of the refractory elements, i.e. Si, Mg, Fe. They form together with oxygen some very stable compounds with high melting and boiling temperatures. The less abundant elements Al, Ca, Na, Ti, Zr form some condensates which are even more stable than the magnesium-iron-silicon compounds, but their abundances are much too low to form dust in quantities which can easely be detected by a contribution of such dust components to the infrared emission from the circumstellar dust shell. Some of them may, however, be important for the formation of seed nuclei.

For the standard cosmic element mixture numerous calculations of condensation sequences (e.g. Grossman 1972; Lattimer et al. 1978; Saxena & Ericksson 1986; Sharp & Huebner 1990; Lodders & Fegley 1995; Lodders & Fegley 1999; Ebel & Grossman 2000) have shown that in chemical equilibrium forsterite with composition Mg_2SiO_4, enstatite with composition $MgSiO_3$, and free metallic iron are the most stable condensates from the abundant elements. The element mixture used in such

calculations corresponds to a magnesium to silicon abundance ratio for the standard cosmic element mixture of $\epsilon_{\rm Mg}/\epsilon_{\rm Si} = 1.075$, if the latest abundance tabulation of Anders & Grevesse (1989) and Grevesse & Noels (1993) is used, or to some value close to this for other tabular values.

If one considers in a thermodynamic equilibrium calculation that forsterite and enstatite form solid solutions with their iron bearing counterparts, fayalite with composition Fe_2SiO_4 and ferrosilite with composition $FeSiO_3$, respectively, it turns out that in equilibrium not the pure end-members of the two solution series are the stable compounds but that olivine with composition $Mg_{2x}Fe_{2(1-x)}SiO_4$ and pyroxene with composition $Mg_xFe_{1-x}SiO_3$ are formed. However, in chemical equilibrium the iron content is small, i.e. $(1-x) \ll 1$ (e.g. Saxena & Ericksson 1986). We neglect in our following considerations the small quantities of Fe bound in olivine and pyroxene and consider only the pure compounds forsterite and enstatite.

A mixture of forsterite and enstatite is obtained in chemical equilibrium only if the magnesium to silicon abundance ratio satisfies the inequality $1 < \epsilon_{\rm Mg}/\epsilon_{\rm Si} < 2$. In principle forsterite is more stable than enstatite, but forsterite requires two Mg atoms per Si atom for its formation in contrast to enstatite, which requires only one. If $1 < \epsilon_{\rm Mg}/\epsilon_{\rm Si} < 2$ there is insufficient Mg available in the element mixture to condense all Si atoms into the more stable forsterite. In this case some enstatite is formed besides forsterite in such quantities that at low temperatures forsterite and enstatite consume all the available silicon and magnesium.

If $\epsilon_{\rm Mg}/\epsilon_{\rm Si} > 2$, more magnesium is present in the mixture than can be bound in forsterite. No enstatite is formed in this case and the excess magnesium forms some other stable compound, which turns out to be solid MgO, which is well known to be very stable up to high temperatures.

If $\epsilon_{\rm Mg}/\epsilon_{\rm Si} < 1$, insufficient quantities of magnesium are available to condense all the silicon into enstatite. In this case at low temperatures the formation of enstatite consumes all the available magnesium and no forsterite is formed. The left over silicon forms some other stable silicon compound. It turns out that this is quartz in this case, which also is a rather stable compound.

The main features of the mineral mixture formed at different magnesium to silicon abundance ratios are determined by stoichiometric requirements in order to distribute Mg and Si between the most stable (forsterite) and second most stable (enstatite) magnesium-silicon compounds, which consume Mg and Si completely in the abundance ratio interval $1 < \epsilon_{\rm Mg}/\epsilon_{\rm Si} < 2$ of their coexistence. Only outside this region some different Si or Mg bearing compounds may be formed. The further details of the equilibrium condensation have to be determined from a calculation of the equilibrium mineral mixture by the methods of chemical thermodynamics.

The less abundant elements Al and Ca form some very stable solid compounds together with Si, Mg, and O. In the temperature region where forsterite is stable these are mainly spinel ($MgAl_2O_4$) and diopside ($CaMgSi_2O_6$) or anorthite ($CaAl_2Si_2O_8$). Their formation consumes some fraction of the elements Mg and Si which then are not available for the formation of other magnesium and silicon compounds, since these Al and Ca compounds are more stable. This shifts the above mentioned limits for the magnesium to silicon abundance ratio to somewhat lower values, without changing the general picture. We therefore arbitrarily assume for simplicity the Al and Ca to be completely condensed into spinel and diopside and do not consider the details of the Al-Ca chemistry (and of the less abundant elements), since these are unimportant for our purposes.

3.2. Calculation of the equilibrium composition

We calculate the chemical composition of a mixture of solids and gas phase species from two sets of equations: (i) the set of laws of mass action for each of the individual species, and (ii) the constraints set by the abundances of the elements.

For any gaseous or solid chemical compound with composition $A_iB_jC_k...$ the chemical reaction of formation of this particular compound from free atoms of the elements denoted by A, B, C, ... may be written as:

$$iA + jB + kC + ... \longrightarrow A_iB_jC_k... \tag{1}$$

In a state of chemical equilibrium the law of mass action for each of the species reads as follows (Atkins 1994)

$$\frac{a_{A_iB_jC_k...}}{p_A^i p_B^j p_C^k...} = e^{-\Delta G/RT} = K_p(T)\,, \tag{2}$$

where $a_{A_iB_jC_k...}$ is the activity of the compound $A_iB_jC_k...$ and ΔG is the change of free enthalpy in the formation of the compound from free gaseous atoms. p_A, p_B, p_C, ... are the gas phase partial pressures of the free atoms of the elements A, B, C, ...

If $A_iB_jC_k...$ is a molecule from the gas phase, the activity $a_{A_iB_jC_k...}$ equals its partial pressure $p_{A_iB_jC_k...}$ in the chemical equilibrium mixture (Atkins 1994) and we have

$$p_{A_iB_jC_k...} = p_A^i p_B^j p_C^k...\ e^{-\Delta G/RT} \quad \text{(molecules)}. \tag{3}$$

If we have determined the partial pressures p_A, p_B, p_C, ... of the free atoms, the partial pressures of all molecules in the mixture are uniquely determined by Eqs. (3).

If $A_iB_jC_k...$ is a solid, its activity in chemical equilibrium equals unity (Atkins 1994) and we have

$$1 = p_A^i p_B^j p_C^k...\ e^{-\Delta G/RT} \quad \text{(solids)}. \tag{4}$$

This defines a relation between the partial pressures of the free atoms involved in the formation for each of the solids existing in a state of chemical equilibrium. For the solid compounds which are not stable for the given element

mixture and for given pressure P and temperature T, their activity calculated from (2) satisfies

$$a_{\mathrm{A}_i\mathrm{B}_j\mathrm{C}_k\ldots} < 1. \tag{5}$$

Thus, in an equilibrium state the possible solid compounds which may be formed from the given elements at pressure P and temperature T either satisfy $a = 1$, in which case they are present in the mixture, or they satisfy $a < 1$, in which case they are absent from the mixture.

For each of the solids which may condense for a given element mixture we define a degree of condensation f of that compound as the fraction of the nuclei of some key element required for its formation that is bound in this solid. Usually the least abundant of the elements required for the formation of the solid is chosen as the key element. We denote the different elements by an index k. Then we have an equation for the total number of nuclei for each element which is of the form

$$P_{\mathrm{H}}\left(\epsilon_k - \sum_{\substack{\text{all solids } l\\ \text{with element } k}} \nu_{k,l} f_l \epsilon_l\right) = \sum_{\substack{\text{all molecules } j\\ \text{with element } k}} \nu_{k,j} p_j. \tag{6}$$

Here P_{H} is the fictitious partial pressure of H nuclei. $\nu_{k,l}$ is the number of atoms of element k in solid l per atom of the least abundant of its constituents, and ϵ_l the element abundance of this element. $\nu_{k,j}$ is the number of atoms of element k contained in molecule j. The partial pressures p_j of the molecules are expressed by means of the law of mass action (3) by the partial pressures of the free atoms. This set is completed by the equation

$$P = \sum_{\text{all molecules } i} p_i \tag{7}$$

for the total pressure P.

The set of Eqs. (6) and (7) together with an equation of the form (2) for each of the solids is subject to the condition that for each of the solids the solution of the equations satisfies:

- either $a = 1$ and $f \geq 0$,
- or $f = 0$ and $a < 1$.

The set of equations is solved for a state with given temperature T and pressure P as follows: first we take advantage from the fact that hydrogen and He are much more abundant than any other of the elements, that these two elements do not condense under the conditions encountered in circumstellar shells, and that at the rather low pressures and temperatures of interest only H, H_2, and He are present. Any compound of hydrogen with less abundant elements can be neglected in calculating P_{H} and P. Then we calculate from the subset of equations

$$P = p_{\mathrm{H}} + p_{\mathrm{H}}^2 K_p(\mathrm{H}_2) + p_{\mathrm{He}} \tag{8}$$

$$P_{\mathrm{H}} = p_{\mathrm{H}} + 2p_{\mathrm{H}}^2 K_p(\mathrm{H}_2) \tag{9}$$

$$P_{\mathrm{H}}\epsilon_{\mathrm{He}} = p_{\mathrm{He}} \tag{10}$$

the partial pressure p_{H} and the auxiliary quantity P_{H}. This solution then is used in Eqs. (6) for all other elements.

The remaining set of Eqs. (6) and (2) is solved for the partial pressures of the free atoms of elements C, O, Mg, Si, S, and Fe and for the degree of condensation f of the different possible condensates formed from these elements. All other elements are not important for the problem of determining the mixture of abundant minerals in chemical equilibrium for M-star abundances, except that we have assumed that some fraction of Si and Mg is consumed by complete condensation of Al and Ca into spinel and diopside. The equations are solved numerically by Newton-Raphson iteration.

Polynomial approximations for calculating ΔG for the formation of molecules and solids from free atoms are taken from Sharp & Huebner (1990). For a number of molecules and solids not contained in that list polynomial approximations for ΔG are taken from Tsuji (1973) or polynomial approximations of the type used by Sharp & Huebner have been calculated from data taken from the JANAF tables (Chase 1985). The error in the JANAF data for HS detected by Ebel & Grossman (2000) has been corrected.

3.3. Results for the mineral mixture

The results for the mineral composition formed in chemical equilibrium for different magnesium to silicon abundance ratios are shown in Fig. 2. The total gas pressure is assumed to equal $P = 10^{-4}\,\mathrm{dyn\,cm^{-2}}$ which is representative for the gas pressure in the condensation zone of circumstellar dust shells (cf. Fig. 7 of Paper I, for instance). Element abundances are those given by Anders & Grevesse (1989) and Grevesse & Noels (1993) except that we have varied the Mg/Si ratio between the limits $0.6 \leq \epsilon_{\mathrm{Mg}}/\epsilon_{\mathrm{Si}} \leq 2.4$, which encompasses the region of Mg/Si ratios which may occur in AGB stars.

The inset in Fig. 2 shows the stability limits and the regions of existence for the different Mg-Si-condensates. Forsterite is the most stable compound at any Mg/Si abundance ratio and the uppermost line corresponds to its stability limit. Above this limit, none of the abundant Mg-Si condensates exists, but only the much less abundant Al-Ca-condensates. The upper stability limit of enstatite occurs at a slightly lower temperature. Enstatite and forsterite coexist in the abundance ratio interval $1 \lesssim \epsilon_{\mathrm{Mg}}/\epsilon_{\mathrm{Si}} \lesssim 2$ at all temperatures below the stability limit of enstatite, and they coexist in the abundance ratio region $\epsilon_{\mathrm{Mg}}/\epsilon_{\mathrm{Si}} \lesssim 1$ only in a small temperature strip just below the stability limit of enstatite. The forsterite disappears in the region $\epsilon_{\mathrm{Mg}}/\epsilon_{\mathrm{Si}} \lesssim 1$ at a certain limit temperature because enstatite takes up all the available Mg below that limit.

In the abundance ratio region $\epsilon_{\mathrm{Mg}}/\epsilon_{\mathrm{Si}} \lesssim 1$ quartz is formed since only part of the Si can be bound in enstatite. Because of the significantly less stability of quartz as compared to the magnesium silicates, the upper stability limit of quartz appears approx. 30 K below the limit where forsterite disappears, such that there is a small

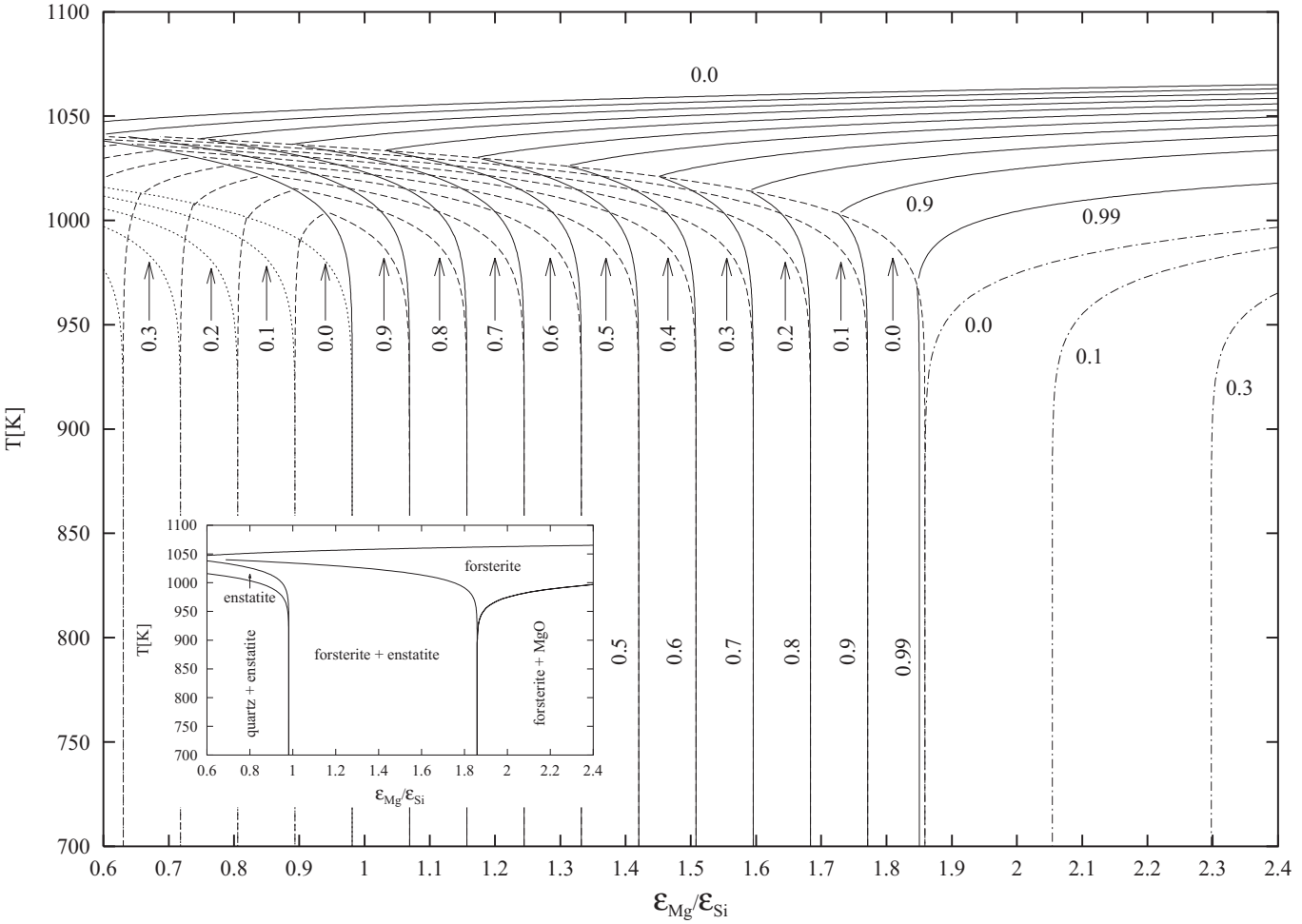

Fig. 2. Lines of constant degree of condensation f of the abundant magnesium and silicate compounds at $P = 10^{-4}\,\mathrm{dyn\,cm^{-2}}$ and varying abundance ratio of magnesium to silicon. *Full lines:* forsterite. *Dashed lines:* enstatite. *Dotted lines:* quartz. *Dashed dotted lines:* MgO. The numbers at the lines denote the degree of condensation of the key element (Si for forsterite, enstatite, and quartz; Mg for MgO) in the solid. The inset shows the stability limits of the different condensates and the regions of coexistence of different mineral mixtures. It is assumed that part of the Si and Mg is bound in spinel and diopside

intermediate region where only enstatite exists. In the abundance ratio region $\epsilon_{\rm Mg}/\epsilon_{\rm Si} > 1$ no quartz is present in the equilibrium mineral mixture since Si forms the more stable forsterite and enstatite.

In the abundance ratio region $\epsilon_{\rm Mg}/\epsilon_{\rm Si} \gtrsim 2$ solid MgO is formed since only part of the Mg can be bound in forsterite. MgO then takes up the excess Mg not bound in forsterite.

Figure 2 shows lines of constant degree of condensation f of the abundant dust species between the stability limit $f = 0$ and the limit of nearly complete condensation $f = 0.99$, from which the details of the equilibrium condensation process can be seen. Note that f is defined for a particular condensate such that it describes the fraction of the key element required for its formation which is bound in that condensate. For quartz, forsterite and enstatite the key element is chosen to be Si, for solid MgO this is Mg. Especially it can be seen from Fig. 2 how the silicon and magnesium are distributed between forsterite and enstatite in chemical equilibrium in the region of Mg/Si abundance ratios $1 \lesssim \epsilon_{\rm Mg}/\epsilon_{\rm Si} \lesssim 1.5$ encountered in the majority of stars.

We have not shown the stability limit and degree of condensation of solid iron, since iron condenses independently from the other minerals at a temperature somewhat below that of olivine (see Fig. 2 of Paper I).

In circumstellar grains the iron content usually is different from zero, though its precise value is not well known. Therefore, in the following, we have not to deal with the pure end-members forsterite or enstatite of their respective solution series, but with the iron bearing compounds olivine and pyroxene, respectively.

4. Non-equilibrium dust condensation in a stellar wind

We calculate models for the formation of dust in a spherically symmetric stationary outflow from a nonvariable star. In view of the fact that most cool giants on the AGB are large amplitude regular or semiregular variables where shock waves regularly traverse the outer layers of

the star, this assumption is highly idealistic. A realistic treatment of multicomponent dust formation problems including stellar pulsation, however, is presently not possible, and stationary models such as that which are considered in the following are well suited to study the basic principles of dust formation in circumstellar shells. A comparison of some results of a model calculation (Winters et al. 1997) for a time-dependent model of dust condensation in a carbon star (one dust component) with results for a model based on a stationary outflow shows that the global characteristics of stationary models are not too different from that of models including pulsation, though the details are quite different. Stationary wind models are adequate, however, for the more luminous supergiants where variability is not as important as on the AGB (Le Bertre & Winters 1998).

4.1. The wind model

The model for the stellar wind is the simplified model described in Paper I: we assume the gas to flow with a constant velocity v_0 of the order of the sonic velocity into the dust forming layer of the circumstellar shell as long as the gravitational pull of the star exceeds the radiation pressure on the gas-dust mixture. Once the ratio

$$\Gamma = \frac{L_*}{4\pi\, c\, G\, M_*}\,\kappa \tag{11}$$

of radiative to gravitational acceleration exceeds unity we solve the equation of motion

$$v\frac{\mathrm{d}v}{\mathrm{d}r} = -\frac{GM_*}{r^2}\,(1-\Gamma) \tag{12}$$

for the outflow velocity v subject to the initial condition

$$v = v_0 \quad \text{at} \quad \Gamma(r) = 1. \tag{13}$$

M_* is the stellar mass and L_* the stellar luminosity. Note that Γ varies with distance from the star. In the dust free region one has $\Gamma \ll 1$, after the onset of dust formation Γ rapidly increases to values $\Gamma > 1$.

In the momentum Eq. (12) the pressure gradient is neglected in order to avoid the necessity to integrate through the singular point of the velocity equation, as it is explicitly done for instance in Gail & Sedlmayr (1987). The explicit consideration of the singular point is an unnecessary complication if the details of the dust nucleation process are neglected, as it is done in the present paper.

The mass density in the outflow is calculated from the equation of mass conservation

$$\rho = \frac{\dot{M}}{4\pi\, r^2 v}. \tag{14}$$

$\dot{M}$ is the rate of mass-loss by the stationary outflow.

The parameters of the wind model are M_*, L_*, $\dot{M}$, and v_0. The choice of parameters is dictated by the circumstance, that we consider mass-loss and dust formation on the AGB. In particular we wish to study the consequences of variations of the abundance ratio of Mg to Si on dust formation in circumstellar shells of AGB stars. We assume in our model calculation a stellar mass of $M_* = 1.0\ M_\odot$ which is at the lower end of initial masses of AGB stars but considers that the stars of interest already have lost part of their mass by a massive stellar wind. Severe mass-loss and circumstellar dust shells are observed for AGB stars if their luminosity has increased up to $\gtrsim 10^4\ L_\odot$. In our model calculation we assume $L_* = 1\,10^4\ L_\odot$. The effective temperature of the star is assumed to be $T_{\rm eff} = 2\,500\,\mathrm{K}$. Typical mass-loss rates observed for stars with dust shells cover a wide range. This parameter is varied in the model calculations (see later). The initial velocity v_0 for integrating (12) is set to $1\,\mathrm{km\,s^{-1}}$, which is of the order of the sound velocity in the dust forming layer.

4.2. Extinction by dust

The flux averaged mass extinction coefficient κ in (11) is assumed to be given by

$$\kappa = \kappa_{\rm gas} + \sum_i f_i \kappa_{i,\rm dust}. \tag{15}$$

The contributions $\kappa_{i,\rm dust}$ of all dust species i are approximated by their Rosseland mean opacities. Additionally we have assumed that the contributions of all the species simply add up, which generally is not valid for the Rosseland mean, except in the case of grey extinction. Since the dust extinction in the wavelength region where most of the stellar energy is emitted (around $\approx 1.5\,\mu$m) varies only slowly with wavelength, the dust absorbs nearly grey and the calculation of κ by simply adding up the separate contributions of the different dust species is sufficiently accurate.

The mass extinction coefficient $\kappa_{i,\rm dust}$ for the different dust components is calculated by assuming that the least abundant of the elements required for its formation is completely condensed into this dust species (for silicate dust, for instance, this usually is the element Si). Since generally condensation of the key element into dust is not complete, the extinction coefficient $\kappa_{i,\rm dust}$ has to be multiplied by the fraction f_i of the key element, which really is condensed into dust species i (see Eq. (15)). This f_i is determined by the calculation of dust condensation.

The mass extinction coefficients κ_i for the different dust species are calculated from optical constants as described in Paper I and in Gail (1998). For calculating the extinction by amorphous pyroxene we take data for the complex index of refraction from Henning & Mutschke (1997) for pyroxene with 30% iron content. The result for the Rosseland mean extinction coefficient can be approximated quite accurately by

$$\kappa_{\rm py} = \left[\left(3.773\,10^{-5}\ T^{2.017}\right)^{-2} + \left\{\left(1.5\,10^{6}\ T^{-2.679}\right)^{-2} + \sqrt{\left(8.356\,10^{-4}\,T^{0.7336}\right)^4 + \left(1.261\,10^{-8}\,T^{2.272}\right)^4}\right\}^{-1}\right]^{-\frac{1}{2}}. \tag{16}$$

Similar expression for the other dust components are given in Paper I.

4.3. Temperature

The temperature structure in the dust shell is calculated in the approximation of Lucy (1971, 1976)

$$T^4(r) = \frac{1}{2}T_{\rm eff}^4 \left[1 - \sqrt{1 - \frac{R_*^2}{r^2}} + \frac{3}{2}\tau_{\rm L}\right]. \quad (17)$$

The optical depth $\tau_{\rm L}$ is determined by

$$\frac{{\rm d}\tau_{\rm L}}{{\rm d}r} = -\rho\kappa\frac{R_*^2}{r^2}. \quad (18)$$

κ is the Rosseland mean mass extinction coefficient given by (15). The differential equation for $\tau_{\rm L}$ has to be solved with the boundary condition

$$\lim_{r\to\infty} \tau_{\rm L} = 0. \quad (19)$$

This approximation assumes that there are no differences between the gas temperature and any of the internal lattice temperatures of the different dust species.

4.4. Dust nucleation

Dust condensation generally is a two-step process which starts with the formation of tiny seed nuclei (probably of sizes of the order of a few nm), which serve as growth centres for later growth to macroscopic grains. The materials from which the seed nuclei are formed may either be the same material as the material of the final dust grains (homogeneous dust formation), or the final grains may be formed by growth of some kind of material on seed nuclei of a different composition (heterogeneous dust formation).

Laboratory investigations of presolar carbon grains from carbon stars on the AGB showed that these grains probably all grew by heterogeneous growth on TiC (or ZrC) seed nuclei (Bernatowicz et al. 1996). TiC (ZrC) has an extremely high equilibrium condensation temperature and is likely to condense prior to carbon, since carbon growth kinetically is possible only for much lower temperatures in the region of 900–1000 K (cf. Cherchneff 1998), very different from what chemical equilibrium calculations tell us ($T_{\rm cond} \approx 1600$ K).

The situation with respect to dust formation in M-stars is unclear. Laboratory results for presolar grains of the same type, as they are obtained for grains from C-stars (Bernatowicz et al. 1996), do not exist for grains from oxygen rich AGB stars. It is known since a long time that homogeneous silicate dust formation is not possible and requires the formation of some different kind of seed particle (e.g. Donn 1978; Gail & Sedlmayr 1986). From theoretical considerations it is proposed by Gail & Sedlmayr (1998a, 1998b) that in this case TiO_2 seed nuclei are formed first, which then serve as growth centres for all later condensates. The detailed calculation of the properties of TiO_2 clusters (structures, bond energies, ...) and its application to nucleation in a stellar wind by Jeong (2000) has shown, that this mechanism could really be responsible for dust nucleation in M-stars. The popular hypothesis that condensation occurs on corundum seed nuclei is unfounded since small aluminium clusters have low bond energies and form only at very low temperatures (Chang et al. 1998).

We do not consider in this paper the problem of nucleation but concentrate on the growth process of dust grains formed from the most abundant refractory elements. We assume that these grains all grow on some kind of seed particles which are formed at a temperature above the upper limit temperature of stability of the abundant dust species. The precise nature of these seed nuclei is not specified in our calculation, but they might be TiO_2 seed particles (cf. Gail & Sedlmayr 1998b; Jeong 2000).

4.5. Dust growth

The basic equations for calculating the growth of dust grains and the assumptions on which they rest are discussed in Paper I. Since some modifications are required to treat dust condensation for arbitrary Mg/Si abundance ratios, we briefly discuss the basic equations in the version used in the present model calculation.

In chemical equilibrium the iron content of the Mg-Fe silicates is quite small for temperatures above ≈600 K, at most a few percent (e.g. Saxena & Ericksson 1986), and can be neglected for the purpose of calculating equilibrium abundances of the solids. This is no more true if condensation occurs in a state far from equilibrium. In this case the silicates can take up a considerable fraction of the iron and we have to consider the possibility that olivine and pyroxene with a high content of Fe may be formed in the stellar outflow.

4.5.1. Growth of olivine grains

The olivine with composition $Mg_{2x}Fe_{2(1-x)}SiO_4$ grows by addition of SiO, Mg, Fe to the surface of a grain and by oxidation with water vapour from the gas phase. Other reactive species bearing Si, Mg, Fe, and O have negligible abundances in the gas phase. The magnesium content, described by x, can take any value $0 \le x \le 1$. The thermally most stable composition is a magnesium rich olivine with x close to unity (cf. Fig. 1 in Paper I). The net reaction for olivine formation is

$$2x{\rm Mg} + 2(1-x){\rm Fe} + {\rm SiO} + 3{\rm H_2O} \longrightarrow {\rm Mg_{2x}Fe_{2(1-x)}SiO_4(s)} + 3{\rm H_2}. \quad (20)$$

The rate determining step for the total growth process may either be the deposition of a SiO molecule to the surface, if sufficient Mg and Fe are available to provide totally two Mg^{2+} and Fe^{2+} cations per Si atom to be build into the olivine lattice, or the rate determining step is the addition of Mg and Fe to a growing grain, if these ingredients are rare in the gas phase. The deposition rates

per unit time and surface area for a particle at rest with respect to the gas phase are

$$J^{\rm gr}_{\rm SiO} = \alpha_{\rm SiO} n_{\rm SiO} v_{\rm th,SiO} \quad (21)$$
$$J^{\rm gr}_{\rm Mg} = \alpha_{\rm Mg} n_{\rm Mg} v_{\rm th,Mg} \quad (22)$$
$$J^{\rm gr}_{\rm Fe} = \alpha_{\rm Fe} n_{\rm Fe} v_{\rm th,Fe} \quad (23)$$
$$J^{\rm gr}_{\rm H_2O} = \alpha_{\rm H_2O} n_{\rm H_2O} v_{\rm th,H_2O}. \quad (24)$$

α denotes the sticking coefficient, n is the particle density of the growth species in the gas phase and v is the root mean square thermal velocity of particles of mass m

$$v = \sqrt{\frac{kT}{2\pi m}}. \quad (25)$$

If the rate determining step for silicate growth is SiO addition all other deposition rates adjust to this rate and the growth rate for spherical grains of radius a is

$$\left.\frac{{\rm d}a}{{\rm d}t}\right|_{\rm growth} = V_0 J^{\rm gr}_{\rm SiO}. \quad (26)$$

V_0 denotes the volume of the nominal monomer in the solid. This requires that for each SiO molecule two Mg or Fe atoms (and three H_2O molecules) are deposited from the gas phase, i.e. we must have

$$J^{\rm gr}_{\rm Mg} + J^{\rm gr}_{\rm Fe} \geq 2 J^{\rm gr}_{\rm SiO}. \quad (27)$$

If the deposition rate of Mg and Fe is less than $2J^{\rm gr}_{\rm SiO}$ the addition of SiO and H_2O to the growing grain adjusts to the deposition rate of Mg and Fe and we have

$$\left.\frac{{\rm d}a}{{\rm d}t}\right|_{\rm growth} = V_0 \tfrac{1}{2}\left[J^{\rm gr}_{\rm Mg} + J^{\rm gr}_{\rm Fe}\right]. \quad (28)$$

The vapourisation rate of olivine by thermal decomposition is given by (see Paper I)

$$J^{\rm dec}_{\rm ol} = \alpha_{\rm SiO}\, v_{\rm SiO}\, \frac{p_{v,\rm SiO}}{kT}, \quad (29)$$

where $p_{v,\rm SiO}$ is the partial pressure of SiO molecules in chemical equilibrium between the gas phase and olivine, corresponding to reaction (20). The change of particle radius by this process is

$$\left.\frac{{\rm d}a}{{\rm d}t}\right|_{\rm vapourisation} = -V_0 J^{\rm dec}_{\rm SiO}. \quad (30)$$

The total change of particle radius is given by the sum of (26) and (30) or by the sum of (28) and (30), depending on whether (27) is satisfied or not, i.e., we have

$$\frac{{\rm d}a}{{\rm d}t} = V_0 \left(J^{\rm gr}_{\rm ol} - J^{\rm dec}_{\rm ol}\right) \quad (31)$$

where the growth rate of olivine is

$$J^{\rm gr}_{\rm ol} = \min\left(J^{\rm gr}_{\rm SiO},\ \tfrac{1}{2}\left[J^{\rm gr}_{\rm Mg} + J^{\rm gr}_{\rm Fe}\right]\right). \quad (32)$$

The equation for the magnesium content x of the olivine is as in Paper I

$$\frac{{\rm d}x}{{\rm d}t} = \frac{3V_0}{a}\left[(x_g - x)\ J^{\rm gr}_{\rm ol} + \tfrac{1}{2}\left(J^{\rm ex}_{+} - J^{\rm ex}_{-}\right)\right]. \quad (33)$$

The rate of exchange of Fe by Mg per unit surface area during collisions of Mg with the grain surface is

$$J^{\rm ex}_{+} = n_{\rm Mg}\, v_{\rm th,Mg}\, \alpha^{\rm ex}. \quad (34)$$

$\alpha^{\rm ex}$ describes the probability of exchange of a Fe lattice atom at the surface by a Mg atom from the gas phase during the scattering process. The rate for the reverse reaction is

$$J^{\rm ex}_{-} = n_{\rm Fe}\, v_{\rm th,Fe}\, \beta^{\rm ex}. \quad (35)$$

In chemical equilibrium we have $J^{\rm ex}_{+} = J^{\rm ex}_{-}$ from which it follows

$$\beta^{\rm ex} = \alpha^{\rm ex} \frac{v_{\rm th,Mg}}{v_{\rm th,Fe}} \frac{n_{\rm Mg,eq}}{n_{\rm Fe}}. \quad (36)$$

The effective exchange rate then is

$$J^{\rm ex}_{+} - J^{\rm ex}_{-} = v_{\rm th,Mg}\, \alpha^{\rm ex} \left(n_{\rm Mg} - n_{\rm Fe} K_{\rm p}(T,x)\right). \quad (37)$$

$K_{\rm p}$ is defined by

$$\frac{p_{\rm Mg}}{p_{\rm Fe}} = {\rm e}^{-\Delta G/RT} = K_{\rm p}(T) \quad (38)$$

as in Paper I.

These equations form our model for the growth of olivine grains from the gas phase. As we have discussed above, we assume that the grains grow on some kind of pre-formed seed nuclei. We then integrate the coupled system of equations for the particle radius a of olivine grains and their composition x starting at that point where $J^{\rm gr}$ exceeds $J^{\rm vap}$ for olivine.

4.5.2. Growth of pyroxene grains

The growth of pyroxene has not been considered in Paper I. The equations determining the growth of this species are obtained in complete analogy to the case of olivine formation.

The pyroxene with composition $Mg_xFe_{1-x}SiO_3$ grows by addition of SiO, Mg, Fe to the surface and by oxidation with water vapour from the gas phase. The magnesium content, described by x, can take any value $0 \leq x \leq 1$. The thermally most stable composition is a magnesium rich pyroxene with x close to unity, as in the case of olivine. The net chemical reaction for pyroxene formation is

$$x{\rm Mg} + (1-x){\rm Fe} + {\rm SiO} + 2{\rm H_2O} \longrightarrow {\rm Mg}_x{\rm Fe}_{(1-x)}{\rm SiO_3(s)} + 2{\rm H_2}. \quad (39)$$

If the rate determining step for pyroxene growth is SiO addition, as in the case of olivine, we have in complete analogy to the previous case

$$\frac{{\rm d}a}{{\rm d}t} = V_0 \left(J^{\rm gr}_{\rm py} - J^{\rm dec}_{\rm py}\right), \quad (40)$$

where the growth rate of pyroxene is

$$J^{\rm gr}_{\rm py} = \min\left(J^{\rm gr}_{\rm SiO},\ \left[J^{\rm gr}_{\rm Mg} + J^{\rm gr}_{\rm Fe}\right]\right). \quad (41)$$

The equation for the magnesium content x of pyroxene is

$$\frac{\mathrm{d}x}{\mathrm{d}t} = \frac{3V_0}{a}\,\left[(x_g - x)\;J^{\rm gr}_{\rm py} + \left(J^{\rm ex}_{+} - J^{\rm ex}_{-}\right)\right]. \tag{42}$$

The only modification is that now there appears no factor $\frac{1}{2}$ at the exchange term. The quantities $J^{\rm gr}_{\rm SiO}$, $J^{\rm dec}_{\rm py}$, $J^{\rm ex}_{+}$, and $J^{\rm ex}_{-}$ are defined analogously to the case of olivine.

These equations form our model for the growth of pyroxene grains from the gas phase. As we have discussed above, we assume that the grains grow on some kind of pre-formed seed nuclei. We then integrate the coupled system of equations for the particle radius a of pyroxene grains and their composition x starting at that point where for the pyroxene $J^{\rm gr}$ exceeds $J^{\rm vap}$.

4.5.3. Conversion of olivine into pyroxene

There exists the possibility that in a Si rich environment, as it is encountered at the onset of grain growth in the circumstellar shell, the olivine reacts with molecules from the gas phase and is converted into pyroxene. Laboratory experiments on conversion of forsterite to enstatite have shown that this process is likely to be controlled by Mg and Si diffusion through the enstatite layer formed on top of the forsterite (Imae et al. 1993). The experimentally determined diffusion coefficient is

$$D = \exp\left(-\frac{60\,700}{T} + 3.6\right). \tag{43}$$

The characteristic time required to convert a forsterite particle of size a into an enstatite particle is

$$t_{\rm conv} = \frac{a^2}{D}. \tag{44}$$

For a $0.1\,\mu$m sized particle one finds at a temperature of $T = 1000\,$K, representative for the dust forming layer, a time of $t_{\rm conv} = 2\,10^7\,$yr. This is to be compared with the time required for the wind material to traverse the dust forming layer, which is of the order of at most of one year. This type of conversion process of olivine into pyroxene by solid diffusion, though in principle possible, is kinetically strongly forbidden in circumstellar shells.

4.5.4. Growth of quartz, iron, and periclase dust grains

The particle growth of these dust components is treated as in Paper I. The corresponding equations are given in Sect. 5.4 of that paper.

4.5.5. Degree of condensation

The degree of condensation of Si in olivine is determined by

$$f_{\rm ol} = \frac{4\pi(a^3_{\rm ol} - a^3_{0,\rm ol})}{3V_{0,\rm ol}}\,\frac{n_{d,\rm ol}}{\epsilon_{\rm Si}\,N_{\rm H}}. \tag{45}$$

$a_{\rm ol}$ is the particle radius of the olivine grains, $a_{0,\rm ol}$ their initial radius, i.e., the radius of the seed nucleus. $V_{0,\rm ol}$ is the volume of the monomer in the solid and $n_{d,\rm ol}$ is the number of olivine grains. $N_{\rm H}$ is the number of hydrogen nuclei, which is determined from the mass density ρ by

$$N_{\rm H} = \frac{\rho}{(1 + 4\epsilon_{\rm He})m_{\rm H}}. \tag{46}$$

Correspondingly, the degree of condensation of Si in pyroxene is given by

$$f_{\rm py} = \frac{4\pi(a^3_{\rm py} - a^3_{0,\rm py})}{3V_{0,\rm py}}\,\frac{n_{d,\rm py}}{\epsilon_{\rm Si}\,N_{\rm H}} \tag{47}$$

and the degree of condensation of Si in quartz is

$$f_{\rm qu} = \frac{4\pi(a^3_{\rm qu} - a^3_{0,\rm qu})}{3V_{0,\rm qu}}\,\frac{n_{d,\rm qu}}{\epsilon_{\rm Si}\,N_{\rm H}}. \tag{48}$$

The degree of condensation of Fe in iron grains is

$$f_{\rm ir} = \frac{4\pi(a^3_{\rm ir} - a^3_{0,\rm ir})}{3V_{0,\rm ir}}\,\frac{n_{d,\rm ir}}{\epsilon_{\rm Fe}\,N_{\rm H}} \tag{49}$$

and the degree of condensation of Mg in periclase (MgO) is

$$f_{\rm pe} = \frac{4\pi(a^3_{\rm pe} - a^3_{0,\rm pe})}{3V_{0,\rm pe}}\,\frac{n_{d,\rm pe}}{\epsilon_{\rm Mg}\,N_{\rm H}}. \tag{50}$$

These condensation degrees f_i for the five dust species i considered in our calculation are used in (15) to calculate the radiation pressure.

4.5.6. Change of gas phase abundances

For the growth species SiO, Mg, Fe, and H_2O we can assume, that Mg and Fe are present in the gas phase only as free atoms, that Si is present in the gas phase only as SiO (we neglect that a small fraction of Si is present as SiS), and that oxygen is present in the gas phase only as CO, SiO and H_2O.

The particle density of H_2O molecules in the gas phase then is given by

$$n_{\rm H_2O} = \Big[\epsilon_{\rm O} - \epsilon_{\rm C} - (1 + 3f_{\rm ol} + 2f_{\rm py} + f_{\rm qu})\,\epsilon_{\rm Si} - f_{\rm pe}\epsilon_{\rm Mg}\Big] \times N_{\rm H}\,, \tag{51}$$

the particle density of SiO molecules by

$$n_{\rm SiO} = (1 - f_{\rm ol} - f_{\rm py} - f_{\rm qu})\epsilon_{\rm Si}\,N_{\rm H}\,, \tag{52}$$

the particle density of Fe atoms by

$$n_{\rm Fe} = \Big[\epsilon_{\rm Fe}(1 - f_{\rm ir}) - (2(1 - x_{\rm ol})f_{\rm ol} + (1 - x_{\rm py})f_{\rm py})\,\epsilon_{\rm Si}\Big] \times N_{\rm H}\,, \tag{53}$$

and the particle density of Mg atoms by

$$n_{\rm Mg} = \Big[\epsilon_{\rm Mg}(1 - f_{\rm pe}) - (2x_{\rm ol}f_{\rm ol} + x_{\rm py}f_{\rm py})\,\epsilon_{\rm Si}\Big]\,N_{\rm H}. \tag{54}$$

These particle densities are used for calculating the growth rates.

4.5.7. Initial conditions

Solving the equations for the growth of dust grains requires the prescription of initial conditions. Our choice is as follows:

The equations of grain growth are solved from that point on outwards, where the corresponding bulk condensate becomes stable. Since we assume that the grains grow on some pre-formed seed nuclei, we prescribe as initial value for the grain radius the radius of the seed nuclei. This radius is assumed for all dust species to equal 1 nm. The number density of seed nuclei per H nucleus in the wind is assumed for all dust species to equal 10^{-13} since the typical number densities of grains in the outflow from M-stars observationally has been determined to be of the order of a few times 10^{-13} (Knapp 1985).

As initial conditions for solving the Eqs. (33) and (42) for the magnesium content x of olivine and pyroxene, respectively, we choose as in Paper I the solution of the corresponding stationary Eqs. (33) and (42) for $x_{\rm ol}$ and $x_{\rm py}$, respectively.

4.6. Sticking coefficients

The sticking coefficients α for olivine, iron and MgO are chosen as described in Paper I. For pyroxene no experimental value for α could be found; for this reason we arbitrarily used the same sticking coefficient as for olivine, though admittedly there is no special reason why both coefficients should be equal.

For quartz one finds very low sticking coefficients measured by means of evaporation experiments. They all are determined from experiments performed at rather high temperatures (e.g. Hashimoto 1990) and are probably not applicable to SiO_2 vapourisation under circumstellar conditions, where temperatures are much lower.

More recently, experimental results for SiO_2 vapourisation at much lower temperatures in a H_2-CO_2 gas mixture have been presented by Mendybaev et al. (1998). The results labeled with IW-3 in their Fig. 2 seem to be those which are applicable to silica vapourisation under circumstellar conditions, since these results are consistent with the vapourisation rate for low pressures ($p_{\rm H_2O} \to 0$) in their Fig. 3. We calculated a sticking coefficient α for the vapourisation of solid SiO_2 from the relation (cf. Eq. (29))

$$\alpha = \frac{J_{\rm vapourisation,experimental}}{p_{\rm SiO}} \sqrt{2\pi k T m_{\rm SiO}} \tag{55}$$

where $p_{\rm SiO}$ is the partial pressure of the SiO molecule in chemical equilibrium with the solid. This assumes that ejection of a SiO molecule from the surface is the rate determining step for vapourisation. From the three datapoints in Fig. 2 of Mendybaev et al. (1998) we obtain sticking coefficients slightly in excess of 0.2 at temperatures around 1550 K. Extrapolating these down to 1000 K yields a sticking coefficient of 0.07, but the extrapolation procedure is very uncertain. As a compromise we choose in our model calculation for quartz a sticking coefficient of

$$\alpha_{\rm quartz} = 0.1\,, \tag{56}$$

which, however, can only be considered as a crude estimate.

4.7. Element abundances

Element abundances are chosen as in Anders & Grevesse (1989) and Grevesse & Noels (1993) except for He, C, N, and O for which AGB abundances according to Table 1 are used. The Mg abundance is considered to be a free parameter and is varied in the calculations in order to study the effects of different Mg/Si abundance ratios. No attempt is made to calculate models for other metallicities.

5. Results of the model calculation

5.1. Wind model

We have calculated a set models for a stellar wind by solving simultaneously the set of equations for the stellar wind and for the condensation and growth of dust as described in the preceding section. We started the outwards integration at the stability limit where the first of the dust species condensing at the highest temperature starts to condense. In all cases considered the first species to condense was found to be olivine. The calculation then follows the path of a gas parcel on its way out. The initial value of $\tau_{\rm L}$ required for solving (18) was determined by a multiple shooting method until the boundary condition (19) is satisfied. The integrations were done by an Adams-Bashforth solver of third order accuracy (e.g. Golub & Ortega 1992) which requires only one evaluation of the r.h.s. of the equations for each time step. The time step size was controlled by requiring that the most rapidly varying function changes by about 3% in each time step.

The diffusion equation for iron cations in olivine is solved as described in Paper I.

5.2. A wind model for the standard element composition

First we present some results for a wind model with $\dot{M} = 10^{-5}\ M_\odot\,{\rm yr}^{-1}$ and with standard element abundances for M stars on the AGB (cf. Sect. 2) since the inclusion of pyroxene in calculating the non-equilibrium dust mixture is new. Figure 3 shows the degree of condensation of the three most important dust forming elements in M stars.

Figure 3a shows the distribution of Si between the gas phase and the three Si bearing condensates considered in this model calculation: olivine, pyroxene, and quartz. In the standard case with a magnesium to silicon abundance ratio of $\epsilon_{\rm Mg}/\epsilon_{\rm Si} = 1.075$, the most abundant Si bearing species in a non-equilibrium condensation model is olivine while pyroxene is formed in significantly less quantities.

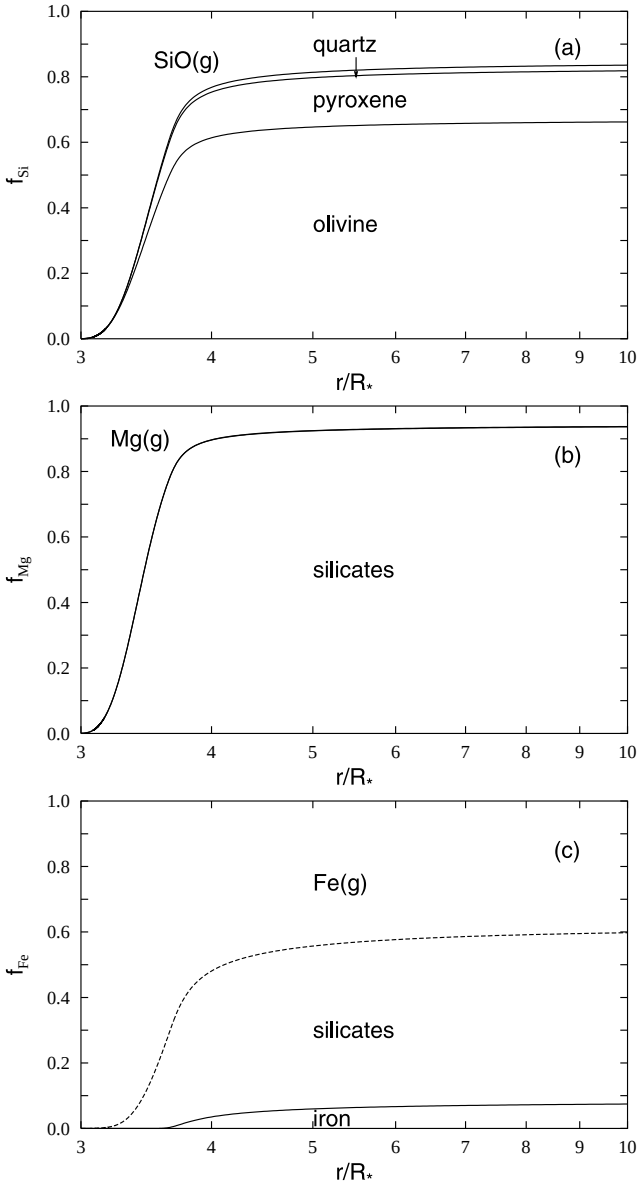

Fig. 3. Distribution of the elements Si, Mg, and Fe between the solid condensates and the gas phase. Wind model with standard element abundances and $\dot{M} = 1\,10^{-5}\ M_\odot\,\mathrm{yr}^{-1}$

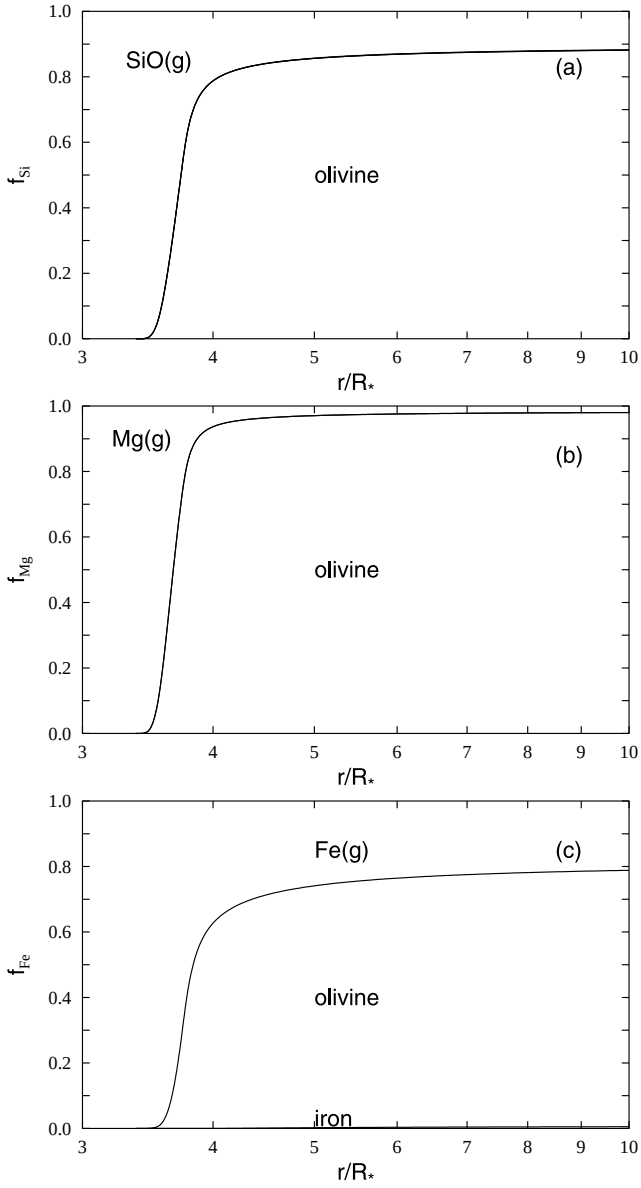

Fig. 4. Distribution of the elements Si, Mg, and Fe between the solid condensates and the gas phase. Wind model with standard element abundances and a high mass loss rate of $\dot{M} = 3\,10^{-5}\ M_\odot\,\mathrm{yr}^{-1}$

This is in sharp contrast to the results of chemical equilibrium calculations where for this element mixture pyroxene would be the dominating condensed silicate species. The reason for this different condensation behaviour in a stellar wind and in the idealised case of chemical equilibrium is the result of two circumstances:

1. Olivine is the more stable one of the two substances and for this reason starts to condense first;
2. Radiation pressure rapidly accelerates the wind material to a highly supersonic outflow velocity once the first strongly absorbing material has condensed to such an extent that Γ, defined by Eq. (11), exceeds unity (this requires a degree of condensation of the order of $f = 0.1$ in case of the silicates).

Since olivine condenses first, the degree of condensation of pyroxene lags somewhat behind that of olivine, though the growth conditions for both substances are similar. The rapid acceleration of the wind, once the degree of condensation of olivine exceeds the limit $f_{\rm ol} \approx 0.1$, rapidly expands and dilutes the wind material. The growth conditions for olivine and pyroxene become unfavourable because of the rapidly decreasing collision rate with growth species from the gas phase and grain growth effectively ceases before the condensible material from the gas phase is exhausted. Under these circumstances pyroxene formation is strongly suppressed. A significant fraction of the silicon is left over as SiO molecule in the gas phase: in a wind model with our present choice of parameters nearly 15% of the silicon.

A small fraction (≈2% in the present model) condenses as quartz. In chemical equilibrium this substance would not be formed in a mixture with the standard Mg/Si abundance ratio since olivine and pyroxene both are more stable than quartz and since sufficient Mg is available to condense the Si completely into these two compounds. During the non-equilibrium condensation process in a stellar wind, however, the quartz first starts to condense at an only slightly lower temperature than olivine. Since during the early phase of the condensation and particle growth process sufficient SiO molecules are available from the gas phase, all silicate compounds grow independently from each other from the gas phase as long as the gas phase remains strongly supersaturated with respect the different condensates.

If the system would evolve towards a chemical equilibrium state, the silicon supply from the gas phase finally becomes exhausted. The partial pressure of SiO in the gas phase drops below the saturation pressure of the least stable species, in this case quartz, and this species then starts to vapourise until it finally disappears in favour of the more stable compounds with a lower saturation pressure of SiO in the gas phase. In this way finally only the most stable compounds survive if the system approaches the chemical equilibrium state. However, this is exactly what does *not* happen in a stellar wind. The evolution towards a chemical equilibrium state is suppressed in a stellar wind because of rapid acceleration of the dusty gas by radiation pressure and the subsequent rapid dilution of the wind material. This freezes some early transition state reached somewhere during the condensation process before the growth species become strongly depleted.

For this reason, a small quantity of quartz can be formed in a stellar wind and this is also the reason why olivine and not pyroxene is the dominating condensed silicate species. Generally, this means, that the results of chemical equilibrium calculations cannot be taken too literally with respect to the existence or non-existence of specific solids, because the dust mixture in circumstellar shells represents a frozen in transition state!

Figure 3b shows the distribution of Mg between the gas phase and the three Mg bearing condensates considered in this model calculation: olivine, pyroxene, and periclase (MgO). According to equilibrium condensation calculations, no periclase is formed in the standard element mixture. In our wind model most of the magnesium is consumed in the formation of the silicates. Periclase is found in the non-equilibrium condensation calculation to be formed in completely negligible quantities. The reason is, that MgO becomes stable only at a temperature where already a significant amount of the Si is condensed in silicates. Growth of significant amounts of solid MgO then is prevented by the rapid dilution of the wind material.

Figure 3c shows the distribution of Fe between the gas phase and the three Fe bearing condensates considered in this model calculation: olivine, pyroxene, and solid iron. The silicates consume only part of the iron, because iron poor silicates are more stable than iron rich silicates. The iron content of the non-equilibrium condensates considerably exceeds the iron content in case of chemical equilibrium, however. Solid iron is formed only in small quatities, since iron starts to condense at a temperature where already significant amounts of silicates are condensed. Again the rapid dilution of the wind material prevents efficient condensation of solid iron.

Figure 4 shows the distribution of elements between the gas phase and solids for a model with a much higher mass loss rate of $\dot{M} = 3\,10^{-5}\ M_\odot\,\mathrm{yr}^{-1}$. In this case only one dust component forms in significant quantities, and this is olivine. Due to its early formation and due to rapid grain growth in the high density wind its formation accelerates the wind material by radiation pressure on grains to supersonic outflow velocities before any other material had a chance to condense in significant amounts. This demonstrates how the early formation of an abundant dust material suppresses any condensation of additional dust species in a stellar wind. Coexistence of significant amounts of more than one dust species seems to be possible only for a not too high mass-loss rates or if an abundant first condensate is only an inefficient absorber for stellar radiation.

5.3. Variation of the dust mixture with varying Mg/Si abundance ratios

Next we consider the dependence of the mineral mixture in the dust shell on the abundance ratio of magnesium to silicon. We concentrate on abundance ratios of $0.6 \le \epsilon_{\mathrm{Mg}}/\epsilon_{\mathrm{Si}} \le 1.5$ since this is the domain of Mg/Si ratios which are likely to occur in AGB stars. In the model calculations the Si abundance is held fixed and the Mg abundance is varied since variations of the Mg/Si ratio are mainly due to the scattering in Mg abundances (cf. Edvardsson et al. 1993). Figure 1 indicates that also somewhat higher abundance ratios may be found and for one star a ratio slightly exceeding a value of two is found, but one may doubt whether such high Mg/Si abundance ratios are real.

Figure 5 shows the results of model calculations for a set of wind models with varying Mg/Si abundance ratios and a fixed mass-loss rate of $10^{-5}\ M_\odot\,\mathrm{yr}^{-1}$. The radial variation of the degree of condensation of the most abundant dust components olivine, pyroxene, solid iron and quartz is shown for different values of $\epsilon_{\mathrm{Mg}}/\epsilon_{\mathrm{Si}}$. The relative abundance of these dust components is quite different from what is expected from equilibrium calculations.

(a) Considerable amounts of olivine are formed even for $\epsilon_{\mathrm{Mg}}/\epsilon_{\mathrm{Si}} < 1$ though this mineral according to the results of Sect. 3.3 should exist in a small temperature interval just below its stability limit only. The high olivine abundance results from the effect discussed above, that olivine as the most stable silicate is the first of the silicate minerals to condense and this rapidly accelerates the outflowing gas, which prevents the system to evolve into the equilibrium state. The quantities of pyroxene formed increase with decreasing Mg/Si abundance ratio

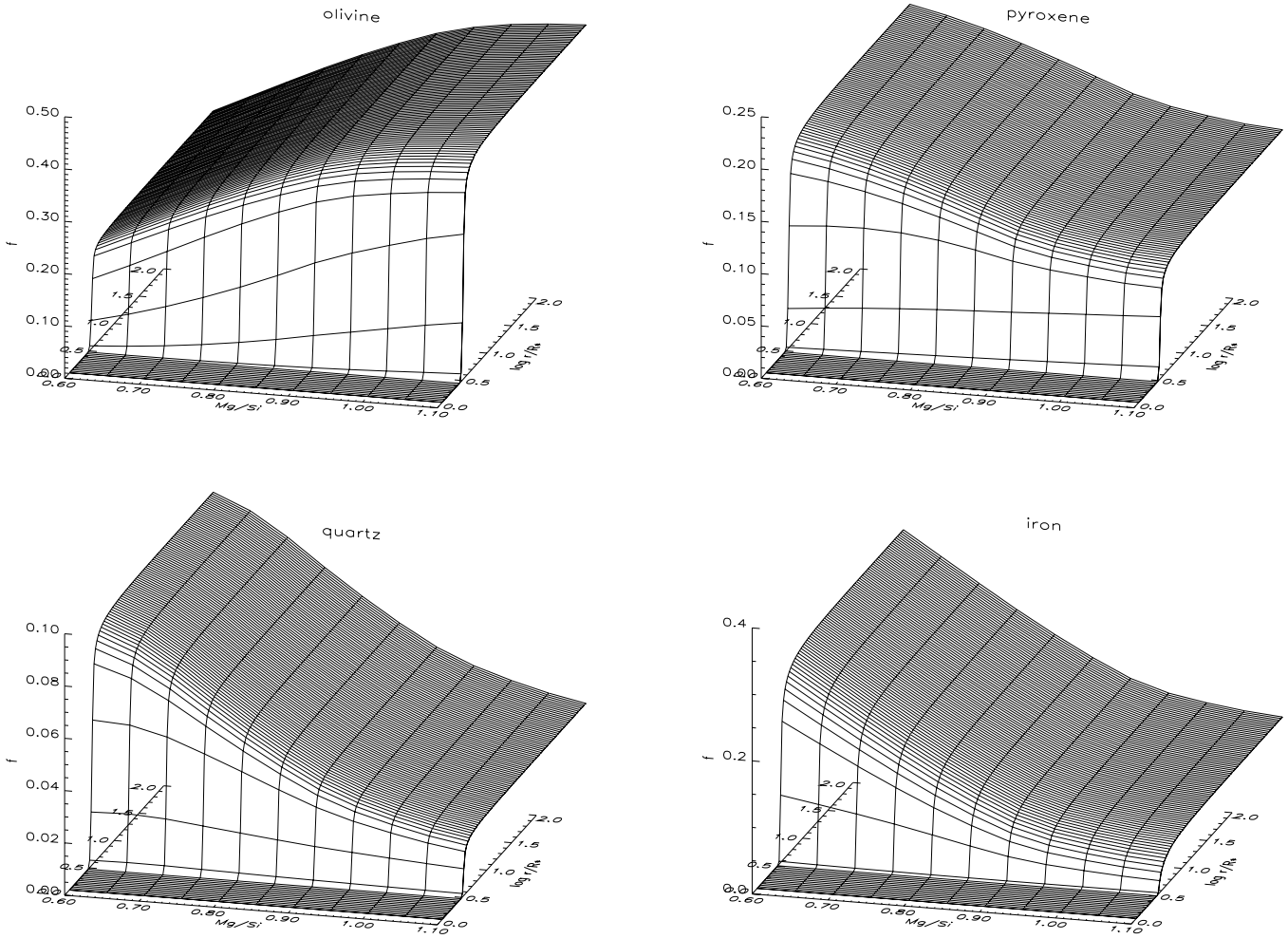

Fig. 5. Radial variation of the degree of condensation f of the abundant dust components for different Mg/Si abundance ratios for a stellar wind model with $\dot{M} = 10^{-5}\ M_\odot\ \mathrm{yr}^{-1}$

for $\epsilon_{\mathrm{Mg}}/\epsilon_{\mathrm{Si}} < 1$, but pyroxene never is the dominating magnesium-silicate dust species for $\epsilon_{\mathrm{Mg}}/\epsilon_{\mathrm{Si}} < 1$, as suggested by chemical equilibrium calculations, because the early formation of olivine and the subsequent wind acceleration by radiation pressure on olivine hampers efficient pyroxene growth.

(b) For $\epsilon_{\mathrm{Mg}}/\epsilon_{\mathrm{Si}} < 1$ quartz is formed as a significant dust component, as is to be expected from the results for the chemical equilibrium condensation. It is, however, not formed in such big quantities as it is suggested by chemical equilibrium. The reason, again, is the early condensation of olivine which reduces the efficiency of condensation of the less stable dust species. In any case, our results show that quartz is formed in such quantities that this mineral should be a detectable dust component in objects with low Mg/Si abundance ratios. This is shown in Sect. 6. The condensation of quartz does not vanish for $\epsilon_{\mathrm{Mg}}/\epsilon_{\mathrm{Si}} > 1$ as in the case of chemical equilibrium, but in this Mg/Si abundance ratio region the quantities of quartz formed in Mg rich objects is very small. The reason that quartz is formed after all is the non-equilibrium effect discussed in the preceding section.

(c) Considerable amounts of metallic iron are formed as a separate dust component in our model calculation. Most of the iron, however, is bound in olivine and pyroxene. Only for the models with lowest Mg/Si abundance ratios more iron is present in form of iron grains than is bound in magnesium-iron-silicates. The increase of the degree of condensation of iron with decreasing $\epsilon_{\mathrm{Mg}}/\epsilon_{\mathrm{Si}}$ results from the decrease in the quantities of olivine formed with decreasing $\epsilon_{\mathrm{Mg}}/\epsilon_{\mathrm{Si}}$ which then less efficiently reduces the efficiency of condensation of the less stable dust species.

Figure 6 shows the radial variation of the degree of condensation f of the different minerals for a magnesium-poor element mixture with $\epsilon_{\mathrm{Mg}}/\epsilon_{\mathrm{Si}} = 0.6$ for wind models with three different mass loss rates. This Mg/Si abundance ratio is at the lowest end of Mg abundances which might occur in stars with population I and II metallicities and represents the most extreme case which possibly can be found in observations.

The top picture of Fig. 6 shows the mineral mixture for a wind model with $\dot{M} = 5\,10^{-6}\ M_\odot\,\mathrm{yr}^{-1}$. In this model the low density of the outflowing gas results in a rather slow growth of dust. The wind then is not yet strongly

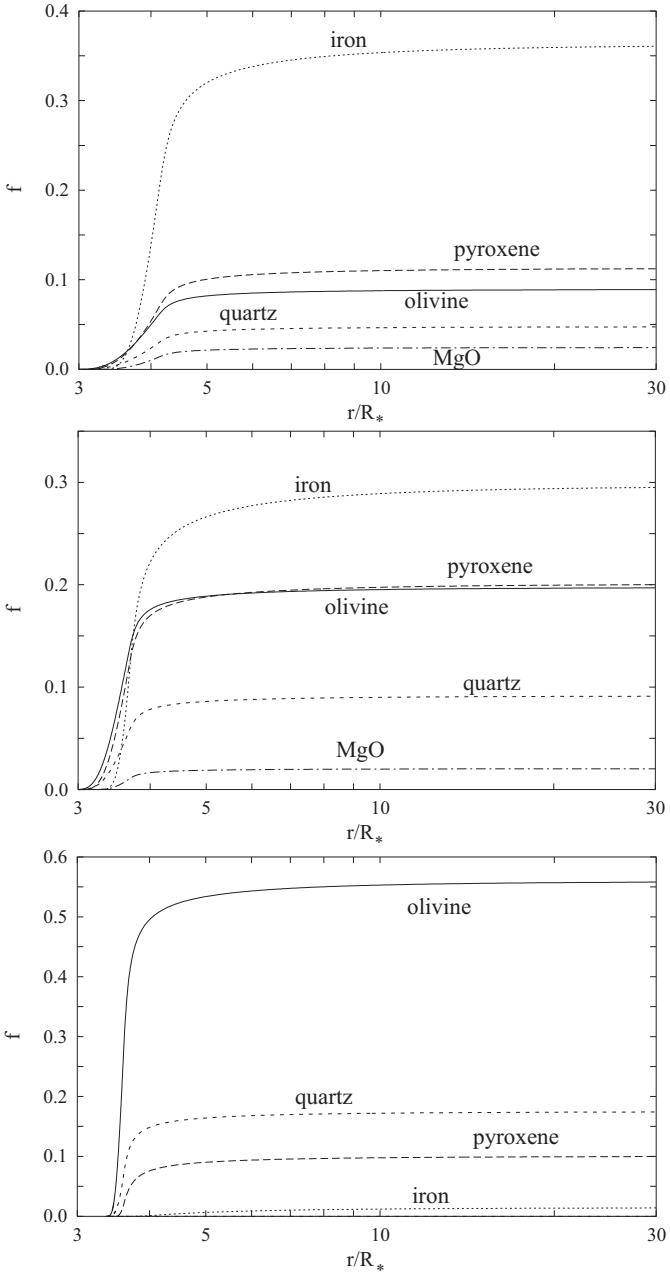

Fig. 6. Radial variation of the degree of condensation f of the abundant dust components for a magnesium-poor element mixture with $\epsilon_{\rm Mg}/\epsilon_{\rm Si} = 0.6$ for stellar wind models with three different mass-loss rates of $\dot{M} = 5\,10^{-6},\ 1\,10^{-5},\ 5\,10^{-5}\ M_\odot\,{\rm yr}^{-1}$ (from top to bottom)

accelerated by radiation pressure on silicate grains once the outflowing material enters the temperature regime where iron condensation becomes possible. The high sticking efficiency near unity typical for growth of metals then results in a much more rapid growth of the iron than of the other mineral species. As a result, radiation pressure on iron dust and subsequent strong acceleration of the wind material then hampers the further growth of the other dust components.

The middle picture of Fig. 6 shows the mineral mixture for a wind model with $\dot{M} = 1\,10^{-5}\ M_\odot\,{\rm yr}^{-1}$. It shows in a different way the mineral mixture also shown in Fig. 5.

The bottom picture of Fig. 6c shows the mineral mixture for a wind model with $\dot{M} = 5\,10^{-5}\ M_\odot\,{\rm yr}^{-1}$. The rather fortunate growth conditions in a high-mass-loss wind favours rapid grain growth and especially the early growth of olivine. The olivine then is the most abundant mineral which forms first and hampers efficient growth of the less stable minerals. Nevertheless pyroxene and quartz are formed in non-negligible quantities. The formation of iron grains, however, is efficiently suppressed because of the lower condensation temperature of iron. If the outflowing gas enters the temperature regime where iron becomes stable, the preceding formation of the other dust species has accelerated the wind to such an extent, that efficient dust growth is no more possible.

These explorative model calculations show that in a certain fraction of giant stars of spectral type M on the AGB, where magnesium is less abundant than silicon, one expects quartz grains to be formed besides the two standard silicate dust components olivine and pyroxene.

A word of warning is appropriate at this place. Our results for the relative amounts of the different dust species formed in the wind depend to a large extent on the numerical values accepted for the sticking coefficients, which are not well known, except perhaps that of iron (for pure metals one generally has $\alpha = 1$). Especially we did not succeed in finding experimental results for the sticking coefficient of pyroxene and, for this reason, assumed this to equal that of olivine, which may be not true. The relative amounts of olivine and pyroxene formed in a real dust shell may be different from what we have found in our model calculation if the two sticking coefficients are strongly different from each other. The same caveat holds with respect to the relative amounts of quartz and silicates formed in the wind.

6. Infrared spectra from the dust shell

In order to study the possibility that quartz grains may be detected by their characteristic extinction bands from circumstellar spectra in the presence of other silicates we have calculated IR emission spectra for our wind models. These are obtained by solving the equation of radiative transfer in a spherically symmetric dust shell by the p-z-method and the method of Feautrier as described by Mihalas (1978). The temperature distribution was taken from the solution of the wind model. This does not consider the possibility that the dust temperatures may be different for different dust species and limits to some extent the accuracy of the calculated spectra. It was not attempted to obtain a completely self consistent solution for the wind model and the radiative transfer problem. The scattering by grains is included by a fixed point iteration method and assuming an angular distribution of the scattered radiation as for dipole scattering (small particle limit).

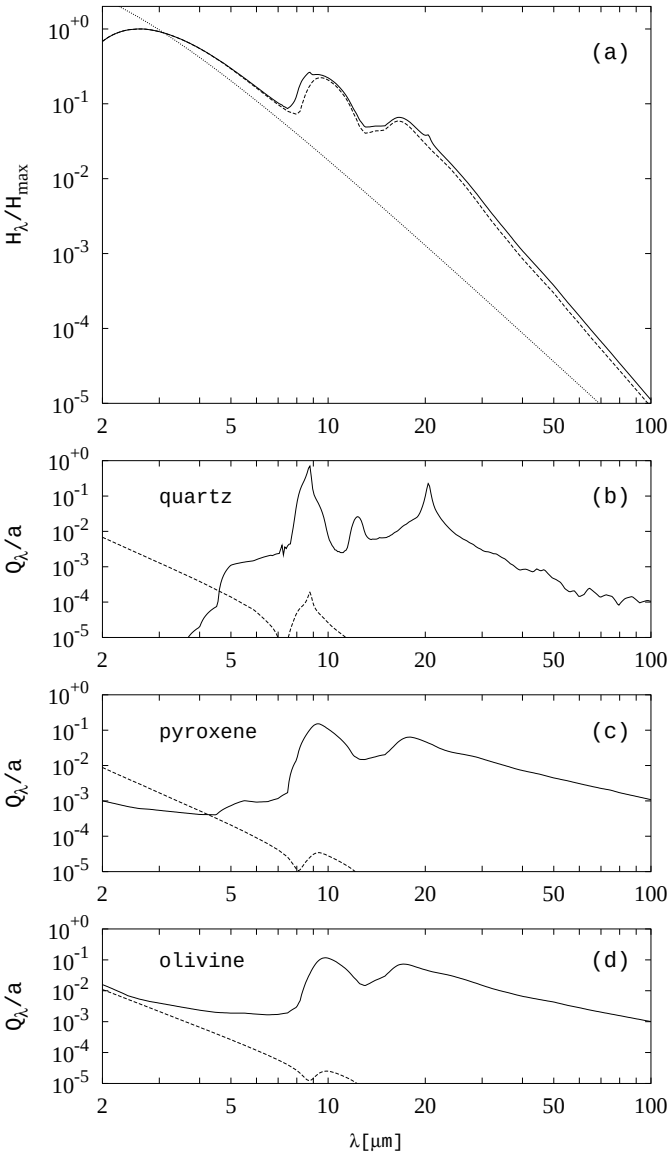

Fig. 7. a) Spectral energy distribution of the dust shell for a model with $\dot{M} = 1\,10^{-5}\ M_\odot\,\mathrm{yr}^{-1}$ for $\epsilon_{\rm Mg}/\epsilon_{\rm Si} = 0.8$. *Full line:* spectral energy distribution including extinction by quartz. *Dashed line:* spectral energy distribution neglecting extinction by quartz. *Dotted line;* The stellar black-body spectrum. **b)** Q_λ/a for absorption (full line) and scattering (dashed line) of amorphous quartz, **c)** the same for amorphous pyroxene, and **d)** for amorphous olivine

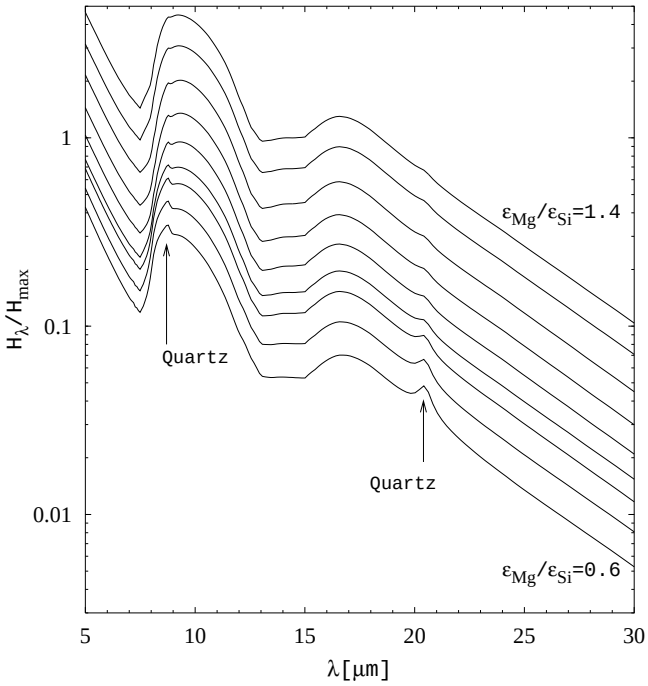

Fig. 8. Variation of the spectral energy distribution of the dust shell (in arbitrary units) with varying Mg/Si abundance ratio for a model with $\dot{M} = 1\,10^{-5}\ M_\odot\,\mathrm{yr}^{-1}$ and Mg/Si abundance ratios between 0.6 (lowest spectrum) and 1.4 (uppermost spectrum) in steps of 0.1. The individual spectra are vertically shifted by a factor of 1.5 each. The two spectral features of quartz at $\lambda \approx 8.7\,\mu$m and $\lambda \approx 20.5\,\mu$m can clearly be seen in the spectrum for $\epsilon_{\rm Mg}/\epsilon_{\rm Si} \lesssim 1$

The radiation of the central star was approximated by a black body of temperature $T_{\rm eff}$. At the outer boundary of the shell the influx of interstellar radiation was chosen as that given by the model of Mathis et al. (1983).

The inner boundary of the dust shell is determined by the condensation calculation and depends on $T_{\rm eff}$ and to some extent on $\dot{M}$. For an assumed $T_{\rm eff} = 2500\,$K it is located at about 3 R_* (cf. Fig. 6). The outer boundary is always assumed to be located at 1000 R_*.

For calculating the extinction of the dust grains we use optical constants for amorphous silicate dust grains (cf. Sect. 4.2): (i) for glassy quartz from Brewster (1992) for the short and from Henning & Mutschke (1997) for the long wavelength region, (ii) for amorphous olivine from Dorschner et al. (1995), (iii) for amorphous pyroxene from Henning & Mutschke (1997), (iv) for iron from Lide (1995) and Pollack et al. (1994). The grain radius used for the calculation of the absorption and scattering efficiencies Q_λ is the grain radius resulting from the wind model[1]. Since the grain radii vary with distance from the star, the extinction efficiencies Q_λ have to be calculated for each radius in the dust shell and each wavelength grid point used in the model calculation ($\approx 160 \times 390$). For reasons of computational efficiency these are calculated in the approximation of small grains, which is always valid in the far IR wavelength region, in which we are interested.

Figure 7a shows the resulting spectral energy distribution of the dust shell for a wind model in the wavelength region $2 \le \lambda \le 100\,\mu$m, where a number of absorption bands of quartz exist. The model is calculated with a Mg/Si abundance ratio of 0.8 and a mass-loss rate of $1\,10^{-5}\ M_\odot\,\mathrm{yr}^{-1}$ for which about 7% of the Si is expected to condense into quartz (cf. Fig. 5). For this mass-loss rate the dust absorption bands appear in the spectrum as emission features. The full line corresponds to

[1] Note, that we assumed grain growth on pre-formed seed nuclei. If nucleation and grain growth are spatially separated, one obtains a nearly monodispersed size spectrum!

the spectral energy distribution of the dust shell including all dust species, the dashed line is the spectral energy distribution obtained if the extinction by quartz is omitted. Figs. 7b, 7c, and 7d show for comparison the absorption and scattering efficiencies Q_λ of quartz, pyroxene and olivine grains with radius 0.1 μm, respectively. Extinction by quartz produces two specific signatures in the spectrum:

- The short wavelength shoulder of the $\lambda \approx 9.7\,\mu$m silicate emission band is significantly widened and steepened by the contribution of the $\lambda \approx 8.7\,\mu$m emission band of quartz;
- The $\lambda \approx 20.5\,\mu$m absorption band of quartz produces a small emission peak at this wavelength superposed on the long wavelength shoulder of the $\lambda \approx 18\,\mu$m silicate emission band.

Additionally, the flat trough between the two strong silicate features is somewhat filled up by quartz emission to the short wavelength side and appears flatter than without quartz. These modifications of the spectral energy distribution should be detectable in observed spectra of circumstellar dust shells, if quartz is present.

Figure 8 shows the spectral energy distributions for a $\dot{M} = 1\,10^{-5}\ M_\odot\,\mathrm{yr}^{-1}$ model for a set of different abundance ratios $0.6 \le \epsilon_{\rm Mg}/\epsilon_{\rm Si} \le 1.4$. For the sake of clarity the individual spectra each are shifted by a constant factor of 1.5 in the vertical direction. This figure clearly shows the variation of the strength of the quartz features with the Mg/Si abundance ratio and how the quartz features become invisible for $\epsilon_{\rm Mg}/\epsilon_{\rm Si} \gtrsim 1$.

In this calculation we have not considered that in many of the dust shells around AGB stars a considerable fraction of the dust is present in a crystalline state (e.g. Waters & Molster 1999). If crystalline dust is present, the dust features are more structured and more pronounced than for amorphous dust. We have calculated spectra for the unfavourable case where dust features are rather diffuse, which in a certain sense is the worst case for finding quartz features.

An inspection of a number of ISO spectra of evolved stars (Molster 2000) shows in some cases weak indications for emission features which might be associated with quartz dust, especially the feature at 20.67 μm. Also the emission band profiles presented by Simpson (1991) seem to show in a few cases weak indications for the presence of quartz. This suggests, that quartz could indeed be found as a dust component in circumstellar shells of highly evolved stars. A definite conclusion can be drawn, however, only on the basis of detailed model calculations for emission from the dust shell and analysis of ISO spectra of possible candidate stars. Because of the uncertainties with respect to the sticking coefficients such calculations should better be done by conventional radiative transfer models for the dust shell where the relative abundances of the different dust species are determined by fitting of observed and synthetic spectra.

7. Concluding remarks

We have studied in this paper the consequences of star-to-star variations of the Mg/Si element abundance ratio on the mineral composition of the dust mixture in dust-shells around AGB stars. For magnesium poor stars with $\epsilon_{\rm Mg} \lesssim \epsilon_{\rm Si}$ it is expected that quartz is formed as an additional dust component which, on the other hand, is absent for stars where $\epsilon_{\rm Mg} > \epsilon_{\rm Si}$. We have shown that sufficient amounts of quartz can be expected to be formed in the Mg-poor stars such that this dust component can be identified by some characteristic spectral features of quartz in the IR spectrum from the dust shell.

The observed element abundances of galactic F and G stars suggest that in a small fraction of all stars of population I and II metallicity, of the order of 10%, the magnesium abundance is less than the silicon abundance. The majority of 90% of all stars have magnesium abundances in excess of the silicon abundance, as it is the case for the sun. For many of these stars, however, the Mg/Si abundance ratio is higher than that given in the abundance tabulation of Anders & Grevesse (1989).

If such stars later evolve to the AGB and develop thick circumstellar dust shells, the Mg-poor stars are likely to form quartz dust grains and a mixture of mainly pyroxene and a smaller quantity of olivine dust grains (and, additionally, iron dust grains), while stars with a normal mixture ($\epsilon_{\rm Mg} > \epsilon_{\rm Si}$) form olivine grains and somewhat less quantities of pyroxene grains, but no quartz grains.

The present day AGB stars inherited their Mg and Si abundances from their main sequence progenitors. One should expect then that the present days AGB stars show the same kind of scattering of Mg/Si abundance ratios as the F and G field dwarf stars, since the average Mg/Si abundance ratio and the extent of scattering in the Mg/Si abundances seems to be roughly independent of the metallicity, except for very low metallicities (cf. Edvardsson et al. 1993; Chen et al. 2000). The dust shells of AGB stars then should show a variable mixture of olivine and pyroxene grains and in a small fraction of all cases quartz dust should be present.

Only one star of the sample of stars shown in Fig. 1 seems to have a magnesium abundance of about twice the silicon abundance. In such an element mixture one expects that solid MgO can be formed as a separate dust component. This high Mg/Si ratio may be an artefact of the errors of the abundance determinations, but if this high ratio should be correct, this means that there exist some stars with MgO dust, but in any case, such objects must be rare.

For very metal poor stars Fig. 1 seems to indicate that magnesium generally is much less abundant than silicon. This would mean that – provided dust condensation is possible in such objects – the very first generations of AGB stars with an oxygen rich chemistry do not form the standard silicate dust grains; they mainly form quartz grains. We have not performed model calculations for this case because our model programme is tailored for dust driven

winds, but for very low metallicities mass-loss cannot be driven by dust condensation.

It should be kept in mind that the quantitative results of the present model calculation for the relative quantities of the different dust species depend on the adopted values of the sticking coefficients which generally are badly known. A better experimental determination of these quantities is urgently required.

Acknowledgements. We acknowledge the constructive criticism of an unknown referee. This work has been performed as part of a project of the special research programme SFB 439 *"Galaxies in the Young Universe"* which is supported by the Deutsche Forschungsgemeinschaft (DFG).

References

Anders, E., & Grevesse, N. 1989, Geochim. Cosmochim. Acta, 53, 197
Atkins, P. W. 1994, Physical Chemistry, 5th Ed. (Oxford University Press)
Barin, I. 1992, Thermodynamical Data of Pure Substances (Verlag Chemie, Weinheim)
Bernatowicz, T. J., Cowsik, R., Gibbons, P. C., et al. 1996, ApJ, 472, 760
Bohren, C. F., & Huffman, D. R. 1983, Absorption and Scattering of Light by Small Particles (John Wiley & Sons, New York)
Brewster, M. Q. 1992, Thermal Radiative Transfer and Properties (John Wiley & Sons, New York etc.)
Chase, M. W. Jr., Davies, C. A., Downey, J. R. Jr., et al. 1985, JANAF Thermodynamic Tables, National Institute of Standards and Technology, Gaithersburg
Chang, C., Patzer, A. B. C., Sedlmayr, E., & Sülzle, D. 1998, Eur. Phys. J. D, 2, 57
Chen, Y. Q., Nissen, P. E., Zhao, G., Zhang, H. W., & Benoni, T. 2000, A&AS, 141, 491
Cherchneff, I. 1998, in The Molecular Astrophysics of Stars and Galaxies, ed. T. W. Hartquist, & D. A. Williams (Clarendon Press, Oxford), 265
Donn, B. 1978, in Protostars & Planets I, ed. T. Gehrels (University of Arizona Press, Tucson), 100
Dorschner, J., Begemann, B., Henning, T., Jaeger, C., & Mutschke, H. 1995, A&A, 300, 503
Ebel, D. S., & Grossman, L. 2000, Geoch. Cosmoch. Acta, 64, 339
Edvardsson, B., Andersen, J., Gustafsson, B., et al. 1993, A&A, 275, 101
Forestini, M., & Charbonnel, C. 1997, A&AS, 123, 241
Gail, H.-P. 1998, A&A, 332, 1099
Gail, H.-P., & Sedlmayr, E. 1986, A&A, 166, 225
Gail, H.-P., & Sedlmayr, E. 1987, A&A, 171, 197
Gail, H.-P., & Sedlmayr, E. 1998a, in The Molecular Astrophysics of Stars and Galaxies, ed. T. W. Hartquist, & D. A. Wiliams (Clarendon Press, Oxford), 285
Gail, H.-P., & Sedlmayr, E. 1998b, Faraday Disc., 109, 303
Gail, H.-P., & Sedlmayr, E. 1999, A&A, 347, 594 (Paper I)
Golub, G. H., & Ortega, J. M. 1992, Scientific Computing and Differential Equations (Academic Press, Boston etc.)
Gratton, R. G., & Sneden, C. 1988, A&A, 204, 193
Grevesse, N., & Noels, A. 1993, in Origin and Evolution of the Elements, ed. N. Prantzos, E. Vangioni-Flam, & M. Cassé (Cambridge University Press, Cambridge), 15
Groenewegen, M. A. T., van den Hoek, L. B., & de Jong, T. 1995, A&A, 293, 381
Grossman, L. 1972, Geochim. Cosmochim. Acta, 36, 597
Hashimoto, A. 1990, Nature, 347, 53
Henning, Th., & Mutschke, H. 1997, A&A, 327, 743
Imae, N., Tsuchijama, A., & Kitamura, M. 1993, Earth Planet. Sci. Lett., 118, 21
Jeong, K. S. 2000, Dust Shells around oxygen-rich Miras and Long-Period Variables, Thesis, Technical University, Berlin
Knapp, G. R. 1985, ApJ, 293, 273
Lang, K. R. 1992, Astrophysical Data, Planets and Stars (Springer, New York etc.)
Lattanzio, J., & Forestini, M. 1999, in Asymptotic Giant Branch Stars, ed. T. Le Bertre, A. Lèbre, & C. Waelkens, IAU Symp., 191 (Astronomical Society of the Pacific), 31
Lattimer, J. M., Schramm, D. N., & Grossman, L. 1978, ApJ, 219, 230
Le Bertre, T., & Winters, J. M. 1998, A&A, 334, 173
Lide, R. D. 1995, CRC Handbook of Chemistry and Physics, 76th Ed. (CRC Press, Boca Raton etc.)
Lodders, K., & Fegley, B., Jr. 1995, Meteoritics, 30, 661
Lodders, K., & Fegley, B. 1999, in ed. T. Le Bertre, A. Lébre, & C. Waelkens, Asymptotic Giant Stars, IAU Symp., 191, 308
Lucy, L. B. 1971, ApJ, 163, 95
Lucy, L. B. 1976, ApJ, 205, 482
Magain, P. 1987, A&A, 179, 176
Mathis, J. S., Mezger, P. G., & Panagia, N. 1983, A&A, 128, 212
Mendybaev, R. A., Beckett, J. R., Grossman, L., & Stolper, E. 1998, Lunar and Planetary Science Conference, 29, 1871
Mihalas, D. 1978, Stellar Atmospheres 2nd Ed. (Freeman, San Francisco)
Molster, F. J. 2000, Thesis, University of Amsterdam
Pollack, J. B., Hollenbach, D., Beckwith, S., et al. 1994, ApJ, 421, 615
Saxena, S. K., & Eriksson, G. 1986, in Chemistry and Physics of Terrestrial Planets, ed. S. K. Saxena (Springer, New York etc.), 30
Schaller, G., Schaerer, D., Meynet, G., & Maeder, A. 1992, A&AS, 96, 269
Sharp, C. M., & Huebner, W. F. 1990, ApJS, 72, 417
Simpson, J. P. 1991, ApJ, 368, 570
Smith, V. V., & Lambert, D. L. 1990, ApJS, 72, 387
Snow, T. P., & Witt, A. 1996, ApJ, 468, L65
Thielemann, F.-K., Nomoto, K., & Hashimoto, M. 1993, in Origin and Evolution of the Elements, ed. N. Prantzos, E. Vangioni-Flam, & M. Cassé (Cambridge University Press, Cambridge), 297
Tomkin, J., Edvardsson, B., Lambert, D. L., & Gustafsson, B. 1997, A&A, 327, 587
Tsuji, T. 1973, A&A, 23, 411
Waters, L. B. F. M., & Molster, F. J. 1999, in Asymptotic Giant Branch Stars, ed. T. Le Bertre, A. Lèbre, & C. Waelkens, IAU Symp., 191, 209
Winters, J. M., Fleischer, A. J., Le Bertre, T., & Sedlmayr, E. 1997, A&A, 326, 305